Supporting Information

for

Discrete Dimers of Redox-Active and Fluorescent Perylene Diimide-Based Rigid Isosceles Triangles in the Solid State

Siva Krishna Mohan Nalluri[†], Jiawang Zhou, [†,‡] Tao Cheng,[‖] Zhichang Liu,[⊥] Minh T. Nguyen,[†] Tianyang Chen,[†] Hasmukh A. Patel,[†] Matthew D. Krzyaniak,[‡] William A. Goddard III,[‖] Michael R. Wasielewski[*†,‡] and J. Fraser Stoddart[*,†,§,#]

[†] *Department of Chemistry, Northwestern University, 2145 Sheridan Road, Evanston, Illinois 60208, USA*
[‡] *Institute for Sustainability and Energy at Northwestern, Northwestern University, 2145 Sheridan Road, Evanston, Illinois 60208, USA*
[‖] *Materials and Process Simulation Center, California Institute of Technology, Pasadena, California 91125, USA*
[⊥] *School of Science, Westlake University, 18 Shilongshan Road, Hangzhou 310024, China*
[§] *Institute for Molecular Design and Synthesis, Tianjin University, 92 Weijin Road, Nankai District, Tianjin 300072, China.*
[#] *School of Chemistry, University of New South Wales, Sydney, NSW 2052, Australia.*

Email: m-wasielewski@northwestern.edu; stoddart@northwestern.edu.

Table of Contents

Section A. Materials / Methods / Instrumentation

All chemicals and reagents were purchased from commercial suppliers (Aldrich or Fisher) and used without further purification. The mono-*N*-Boc protected-*trans*-1,2-cyclohexanediamine derivative **2**,[1] symmetric equilateral triangles [**(−)-3NDI-Δ**[2] and **(−)-3PMDI-Δ**[3]], the compounds (−)-**2PMIA**,[4] **(−)-2NDI-2NH$_2$**,[5] all of the reference molecules — namely, bis(cyclohexyl)perylenetetracarboxylic diimide[6] (**Ref-PDI**), bis(cyclohexyl)naphthalene tetracarboxylic diimide[7] (**Ref-NDI**) and bis(cyclohexyl)pyromellitic diimide[8] (**Ref-PMDI**) — were prepared according to previous literature procedures. Cobaltocene ($CoCp_2$) was handled and stored in an argon Glovebox. While small amounts of (*RR*)-*trans*-1,2-cyclohexanediamine were purchased from Aldrich Chemical Company, larger quantities of the pure enantiomers were obtained by resolving racemic *trans*-1,2-cyclohexanediamine with *L*-(+)-tartaric acid, as described in the literature.[9] Thin layer chromatography (TLC) was performed on silica gel 60 F254 (E. Merck). Column chromatography was carried out on silica gel 60F (Merck 9385, 0.040–0.063 mm). High-resolution mass spectra were measured on an Agilent 6210 Time of Flight (TOF) LC-MS, using an ESI source, coupled with Agilent 1100 HPLC stack, using direct infusion (0.6 mL/min). Nuclear magnetic resonance (NMR) spectra were recorded on a Bruker Avance 600 and Varian P-Inova 500 spectrometers, with working frequencies of 500 and 600 MHz, respectively. Chemical shifts are reported in ppm relative to the signals corresponding to the residual non-deuterated solvents ($CDCl_3$: δ 7.26 ppm).

Photophysical studies and quantum yield measurements. Steady-state UV/Vis absorption spectra were recorded using a UV-3600 Shimadzu spectrophotometer. Solid-state absorption spectra were measured by drop-cast thin films on quartz slides. Diffuse reflectance UV/Vis

measurements were performed using Shimadzu UV-3600 Plus UV/Vis/NIR spectrophotometer equipped with a 150 mm diameter integrating sphere attachment (ISR-1503F). The powder samples were mixed with $BaSO_4$ matrix prior to measurements. Circular dichroism (CD) measurements were carried out on a Jasco J-815 spectrophotometer. Steady-state and time-resolved photoluminescence (TRPL) spectra were acquired using HORIBA Fluorolog-3 equipped with a 450-W xenon lamp and a TCSPC module (diode laser excitation at λ = 375 nm) and an integrating sphere (Horiba Quanta–φ) for absolute photoluminescence quantum yield determination. The spectra were corrected for the monochromator wavelength dependence and photomultiplier response functions provided by the manufacturer. Relative fluorescence quantum yields in solution were measured under high dilution conditions (optical density < 0.05) using *N*,*N*'-dicyclohexylperylene-3,4:9,10-tetracarboxylic acid diimide as a reference compound. Absolute photoluminescence quantum yields in the solid state were measured using (i) as-synthesized powder samples which were placed in a 10 mm diameter holder with a quartz window, as well as (ii) thin film samples which were prepared on quartz slides. All quantum yields were measured in triplicate.

Transient absorption spectroscopy (TA). The 493-nm photoexcitation pulses used in the measurements were obtained through a home-built optical parametric amplifier. The pulse power for photoexcitation was attenuated to ~1 μJ/pulse using neutral density filters. The pump polarization was randomized using a commercial depolarizer (DPU-25-A, Thorlabs, Inc.) to eliminate any orientational dynamics contributions from the experiment. Spectra were collected on a commercial spectrometer (Ultrafast Systems Helios). All solution samples were stirred to avoid localized heating or degradation effects. The optical density was maintained around 0.5 for all samples. Solid-state samples were prepared by drop-cast thin films on quartz slides.

Thermogravimetric analyses (TGA). The studies were carried out under a heating rate of 10 °C min^{-1} up to 800 °C and a nitrogen flow rate of 50 cm^3 min^{-1} using a SDT851 Mettler Toledo Instruments.

Computational Modeling. Quantum mechanics (QM) calculations were carried out on the level of M06-2X density functional[10-11] with 6-311G(d,p) basis sets as implemented in with Jaguar 8.2 (Jaguar, version 8.2, Schrödinger, LLC, New York, NY, 2013).). All the calculations include post-stage D3 van der Waals corrections,[12-13] which we expect to provide accurate descriptions of the non-covalent bonding interactions necessary for **(−)-2PMDI-1PDI-Λ** and **(−)-2NDI-1PDI-**Δ. Solvation effects were considered by using the Poisson-Boltzmann solvation model with parameters of dichloromethane (CH_2Cl_2). The optimized molecular geometries agree well with those in the solid state, but the solvated experimental structures are unavailable. Time-dependent density functional tight binding (TD-DFTB) was employed to predict the UV/Vis absorption spectra.[14] The strain due to the confinement of the triangle scaffold distorted the planar structure of PDI and the calculated structure of the strained PDI was obtained by cutting the C-C bond from the triangle and using hydrogen to saturate the broken bonds We estimated the strain energies by calculating the energy differences between the strained PDIs of both isosceles triangles and fully relaxed monomeric reference PDI compound.

Continuous-wave electron paramagnetic resonance (EPR) and electron-nuclear double resonance (ENDOR) measurements. The spectra were acquired at X-band (9.5 GHz) with a Bruker Elexsys E580 spectrometer, fitted with the DICE ENDOR accessory, an EN801 resonator, and an ENI A-500 RF power amplifier. Applied RF powers ranged from 200 to 400 W across the 7 MHz scanned range, and the microwave power ranged from 2 to 20 mW. EPR Spectra were

recorded with 0.010 mT modulation amplitude. The sample temperatures were controlled by a liquid N_2 flow system. The EPR measurements were carried out on the monoreduced radical anions of the triangles and the reference compound generated by adding 1 mol equiv of cobaltocene ($CoCp_2$) as the chemical reductant. Samples were loaded into 1.4 mm I.D. quartz tubes, which were sealed with epoxy resin in an argon-filled glovebox. A spline fit baseline correction was applied to the ENDOR spectra following integration. The EPR and the ENDOR spectra were fit in MATLAB using EasySpin v4.5.5.

Cyclic Voltammetry (CV) experiments. CV measurements were carried out at room temperature in argon-purged solutions of CH_2Cl_2 with a Gamry Multipurpose instrument (Reference 600) interfaced to a PC. All CV experiments were performed using a glassy carbon working electrode (0.071 cm^2). The electrode surface was polished routinely with 0.05 μm alumina-water slurry on a felt surface immediately before use. The counter electrode was a Pt coil and the reference electrode was an Ag/AgCl electrode. The concentration of the sample and supporting electrolyte, tetrabutylammonium hexafluorophosphate ($TBAPF_6$), were 1.0 mM and 0.1 M, respectively. The CV cell was dried in an oven immediately before use, and argon was continually flushed through the cell as it was cooled down to room temperature to avoid condensation of water.

Spectroelectrochemistry. Spectroelectrochemical measurements were performed using the electrochemical cell arrangement with a platinum mesh as the working electrode, a platinum wire as the counter electrode, and a Ag/AgCl reference electrode. Experiments were carried out in a BASi spectroelectrochemical cell (EF-1362), which was kept continuously under N_2 during the measurements. Absorption spectra were recorded on a UV-3600 Shimadzu spectrophotometer within the UV/Vis/NIR spectral range under several sequentially applied potentials.

Section B. Synthetic protocols

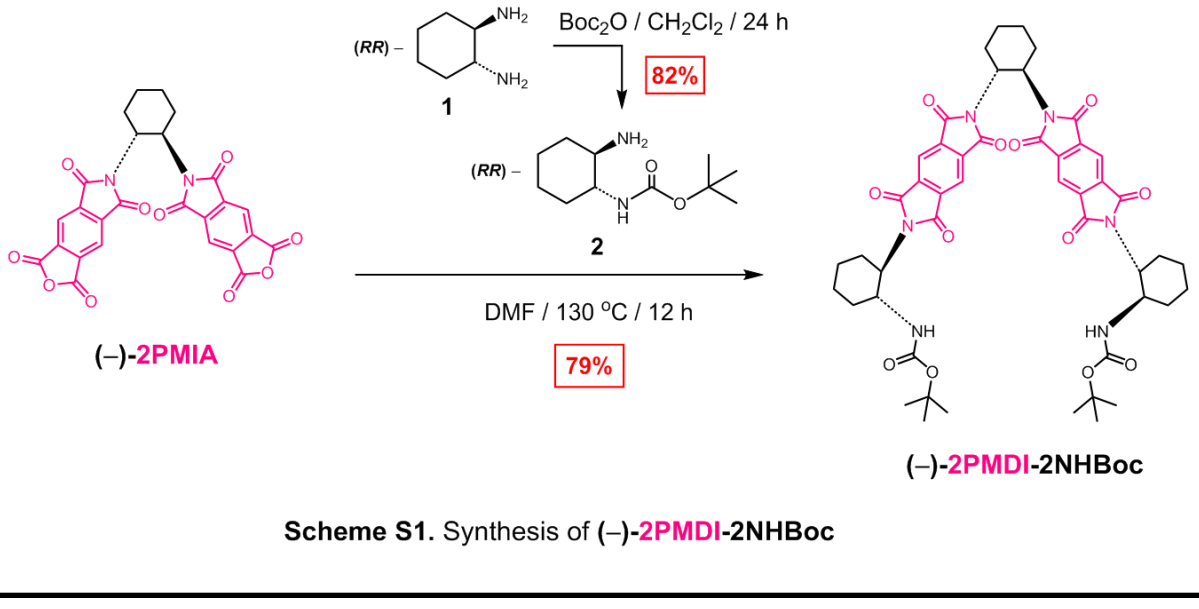

Scheme S1. Synthesis of **(–)-2PMDI-2NHBoc**

(−)-2PMDI-2NHBoc. A solution of compound **2**[1] (535 mg, 2.5 mmol) in anhydrous DMF (10 mL) was added quickly to a vigorously stirred homogenous solution of (−)-**2PMIA**[4] (518 mg, 1.0 mmol) in anhydrous DMF (15 mL) at 70 °C under N_2. The resulting reaction mixture was stirred overnight at 130 °C under N_2, after which the DMF was removed under reduced pressure (~3 mbar) at 60 °C. The crude residue was purified by column chromatography (SiO_2: CH_2Cl_2/Me_2CO, gradient from 0–10% Me_2CO) to afford pure **(−)-2PMDI-2NHBoc** (750 mg, 0.83 mmol) in 79% yield as an off-white powder. ^{1}H NMR (500 MHz, $CDCl_3$, 25 ºC) δ = 8.28 – 7.86 (m, 4H), 4.98 – 4.89 (m, 2H), 4.38 – 4.27 (m, 2H), 4.19 – 4.00 (m, 2H), 3.95 – 3.78 (m, 2H), 2.65 – 2.42 (m, 4H), 2.13 – 0.95 (m, 38H). ^{13}C NMR (125 MHz, $CDCl_3$, 25 ºC) δ = 166.5, 166.1, 155.4, 137.1, 118.3, 79.3, 56.9, 51.8, 50.3, 33.2, 33.0, 28.9, 28.4, 28.1, 28.0, 25.4, 25.4, 25.0, 24.8. ESI-HRMS (*m/z*): calcd for $[M + H]^+$ = 907.3872; found: 907.3845.

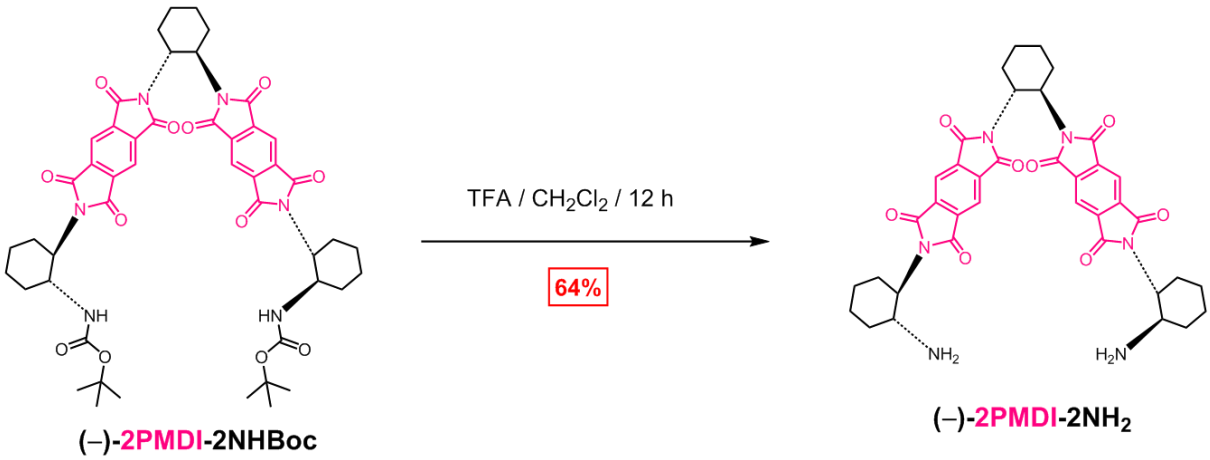

Scheme S2. Synthesis of **(–)-2PMDI-2NH$_2$**

(−)-2PMDI-2NH$_2$. (−)-2PMDI-2NHBoc (750 mg, 0.83 mmol) was dissolved in 1:1 ratio of CH_2Cl_2-trifluoroacetic acid (60 mL) and the solution was stirred at RT for 12 h. The solvent was then evaporated and the crude residue was dispersed in brine (20 mL) and aqueous NH_4OH was added until pH reached 12. The resulting solution was then extracted with CH_2Cl_2 (3 × 30 mL). The organic layers were combined, dried ($MgSO_4$) and concentrated under reduced pressure to afford pure **(−)-2PMDI-2NH$_2$** (374 mg, 0.53 mmol) in 64% isolated yield as a light yellow solid. ^{1}H NMR (500 MHz, $CDCl_3$, 25 ºC) δ = 8.26 – 7.99 (m, 4H), 5.03 – 4.95 (m, 2H), 3.88 – 3.75 (m, 2H), 3.42 – 3.29 (m, 2H), 2.58 – 2.43 (m, 2H), 2.27 – 1.02 (m, 26H). ^{13}C NMR (125 MHz, $CDCl_3$, 25 ºC) δ = 166.7, 166.1, 137.3, 118.5, 118.3, 59.2, 59.0, 51.8, 51.0, 51.0, 37.6, 37.5, 29.5, 29.4, 29.1, 25.7, 25.7, 25.2, 25.2, 25.0. ESI-HRMS (*m/z*): calcd for $[M + H]^+$ = 707.2824; found: 707.2827.

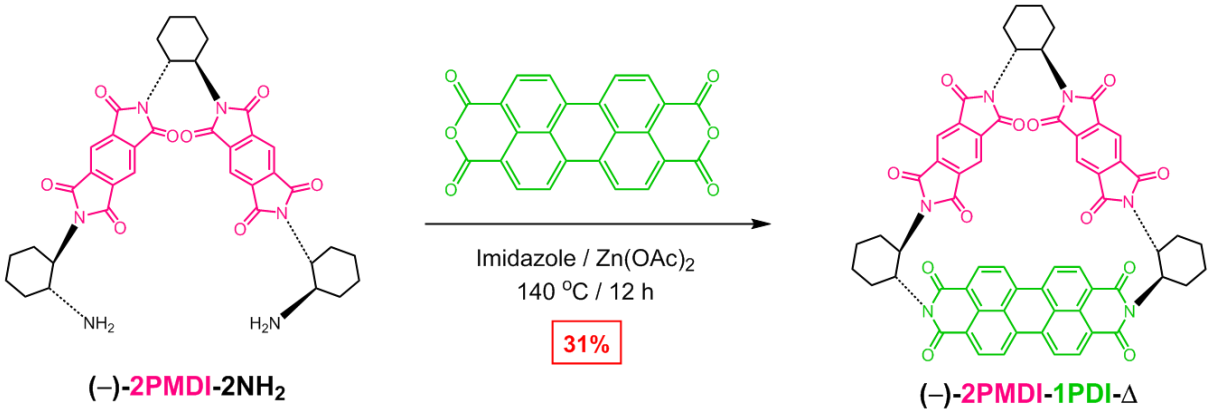

Scheme S3. Synthesis of **(–)-2PMDI-1PDI-Δ**

(−)-2PMDI-1PDI-Δ. The compounds **(−)-2PMDI-2NH$_2$** (226 mg, 0.32 mmol), perylene-3,4:9,10-tetracarboxylic acid bisanhydride (125 mg, 0.32 mmol) and zinc acetate (75 mg, 0.34 mmol) were mixed with imidazole (25 g). The reaction mixture was stirred overnight at 140 °C under N_2. After cooling to room temperature, 1N HCl (200 ml) was added and the resulting solution was extracted with CH_2Cl_2 (3 x 200 ml). The organic layers were combined, dried ($MgSO_4$) and concentrated under reduced pressure. The crude red residue was purified by column chromatography (SiO_2: CH_2Cl_2/Me_2CO, gradient from 0–10% Me_2CO) to afford pure **(−)-2PMDI-1PDI-Δ** (105 mg, 0.099 mmol) in 31% yield as a deep red solid. ^{1}H NMR (500 MHz, $CDCl_3$, 25 ºC) δ = 8.57 (d, *J* = 8.0 Hz, 2H), 8.50 (d, *J* = 8.0 Hz, 2H), 8.45 (overlapped doublets, *J* = 8.0, 7.7 Hz, 4H), 7.83 (s, 4H), 5.80 (td, *J* = 11.7, 3.6 Hz, 2H), 5.42 (td, *J* = 11.8, 3.4 Hz, 2H), 5.24 – 5.16 (m, 2H), 2.64 – 2.52 (m, 2H), 2.24 – 2.13 (m, 4H), 2.02 – 1.91 (m, 6H), 1.85 – 1.75 (m, 6H), 1.75 – 1.60 (m, 4H), 1.5 – 1.39 (m, 2H). ^{13}C NMR (125 MHz, $CDCl_3$, 25 ºC) δ = 166.5, 165.8, 165.8, 165.0, 163.3, 163.2, 137.1, 136.6, 136.5, 136.1, 134.8, 134.4, 132.0, 131.2, 129.1, 126.3, 123.4, 123.3, 123.2, 122.7, 118.4, 118.3, 54.4, 51.7, 51.4, 31.5, 31.1, 30.0, 25.7, 25.6, 24.8. ESI-HRMS (*m/z*): calcd for $[M + H]^+$ = 1063.2933; found: 1063.2917.

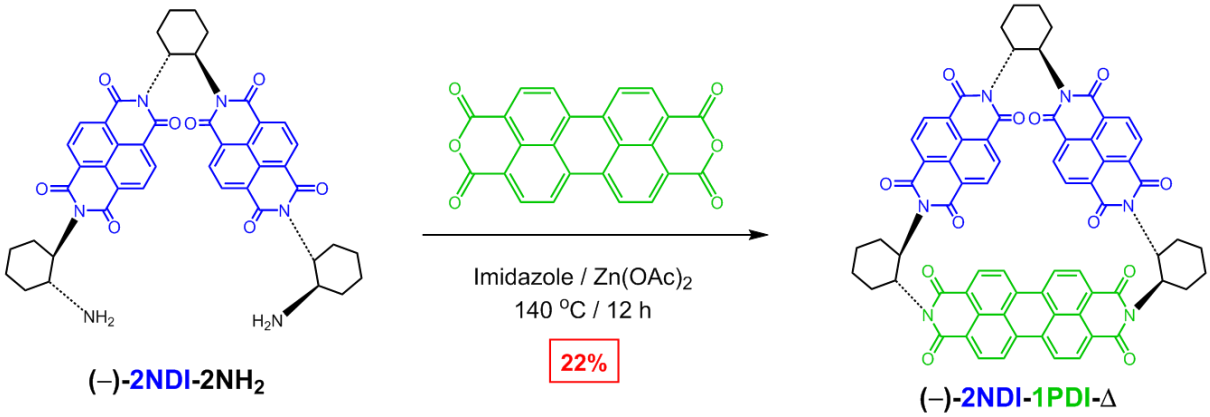

Scheme S4. Synthesis of **(–)-2NDI-1PDI-Δ**

(−)-2NDI-1PDI-Δ. The compounds **(−)-2NDI-2NH$_2$**[5](439 mg, 0.54 mmol), perylene-3,4:9,10-tetracarboxylic acid bisanhydride (214 mg, 0.54 mmol) and zinc acetate (127 mg, 0.58 mmol) were mixed with imidazole (43 g). The reaction mixture was stirred overnight at 140 °C under N_2. After cooling to room temperature, 1N HCl (200 ml) was added and the resulting solution was extracted with CH_2Cl_2 (3 x 200 ml). The organic layers were combined, dried ($MgSO_4$) and concentrated under reduced pressure. The crude red residue was purified by column chromatography (SiO_2: CH_2Cl_2/Me_2CO, gradient from 0–10% Me_2CO) to afford pure **(−)-2NDI-1PDI-Δ** (139 mg, 0.12 mmol) in 22% yield as a bright red solid. ^{1}H NMR (500 MHz, $CDCl_3$, 25 ºC) δ = 8.52 – 8.38 (m, 12H), 8.28 (dd, *J* = 12.7, 8.1 Hz, 4H), 6.44 – 6.35 (m, 2H), 6.23 – 6.11 (m, 4H), 2.70 – 2.57 (m, 2H), 2.51 – 2.37 (m, 2H), 2.37 – 2.25 (m, 2H), 2.20 – 2.12 (m, 2H), 2.05 – 1.93 (m, 6H), 1.88 – 1.67 (m, 8H), 1.63 – 1.58 (m, 2H). ^{13}C NMR (125 MHz, $CDCl_3$, 25 ºC) δ = 163.4, 163.3, 163.2, 162.8, 162.5, 134.2, 134.2, 131.6, 131.4, 131.3, 131.1, 131.0, 130.4, 129.0, 127.0, 126.5, 126.4, 126.3, 126.3, 126.2, 125.8, 123.2, 123.2, 123.0, 122.8, 54.6, 54.4, 54.3, 30.5, 30.3, 30.2, 26.0, 25.6. ESI-HRMS (*m/z*): calcd for $[M + H]^+$ = 1163.3246; found: 1163.3213.

Section C. NMR spectroscopy

a) **^{1}H NMR Spectrum** of **(−)-2PMDI-1PDI-Δ in $CDCl_3$:**

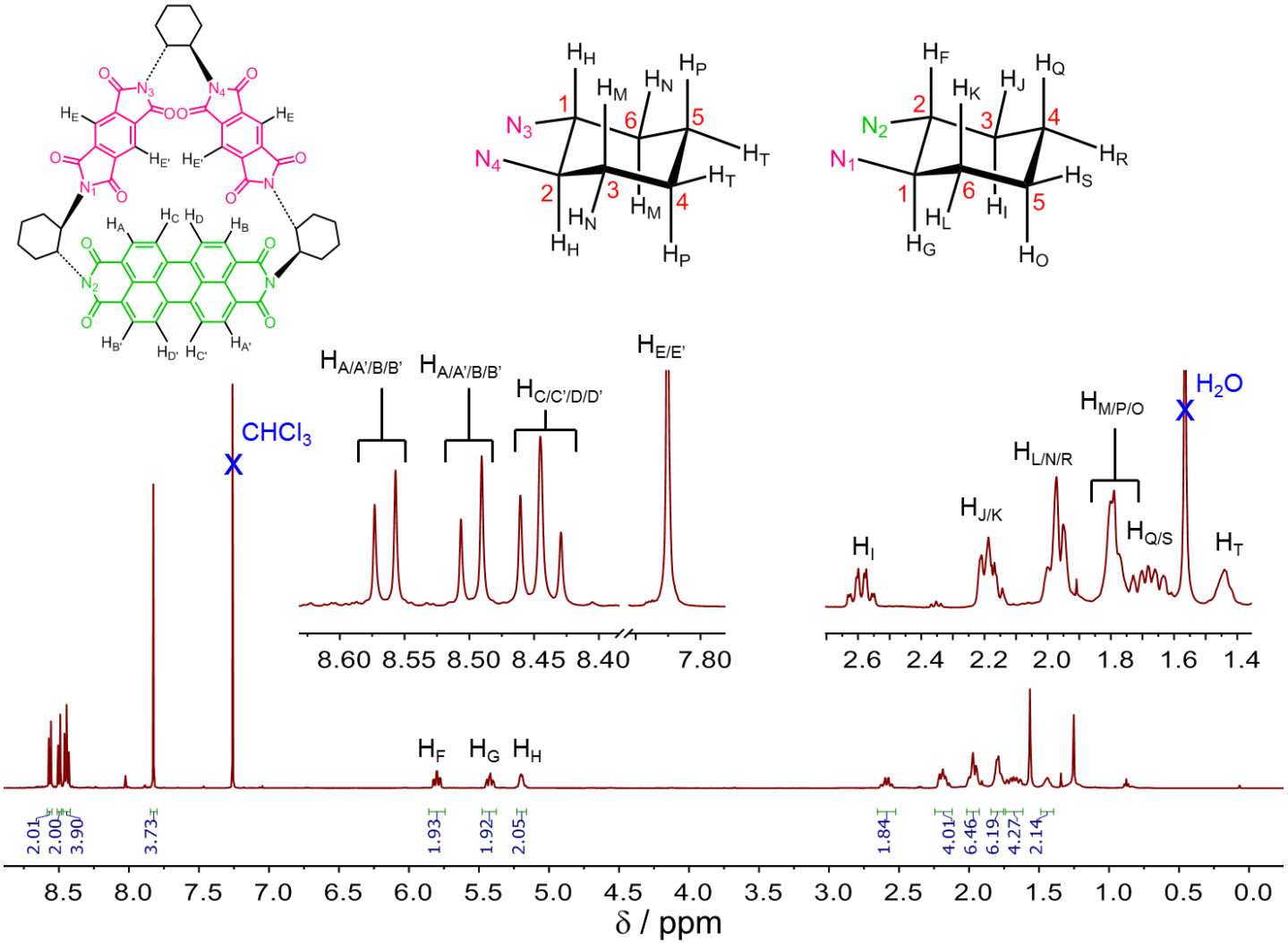

Figure S1. Annotated ^{1}H NMR spectrum (500 MHz, $CDCl_3$, 298 K) of **(−)-2PMDI-1PDI-Δ**.

b) ^{13}C NMR Spectrum of (−)-2PMDI-1PDI-Δ in $CDCl_3$:

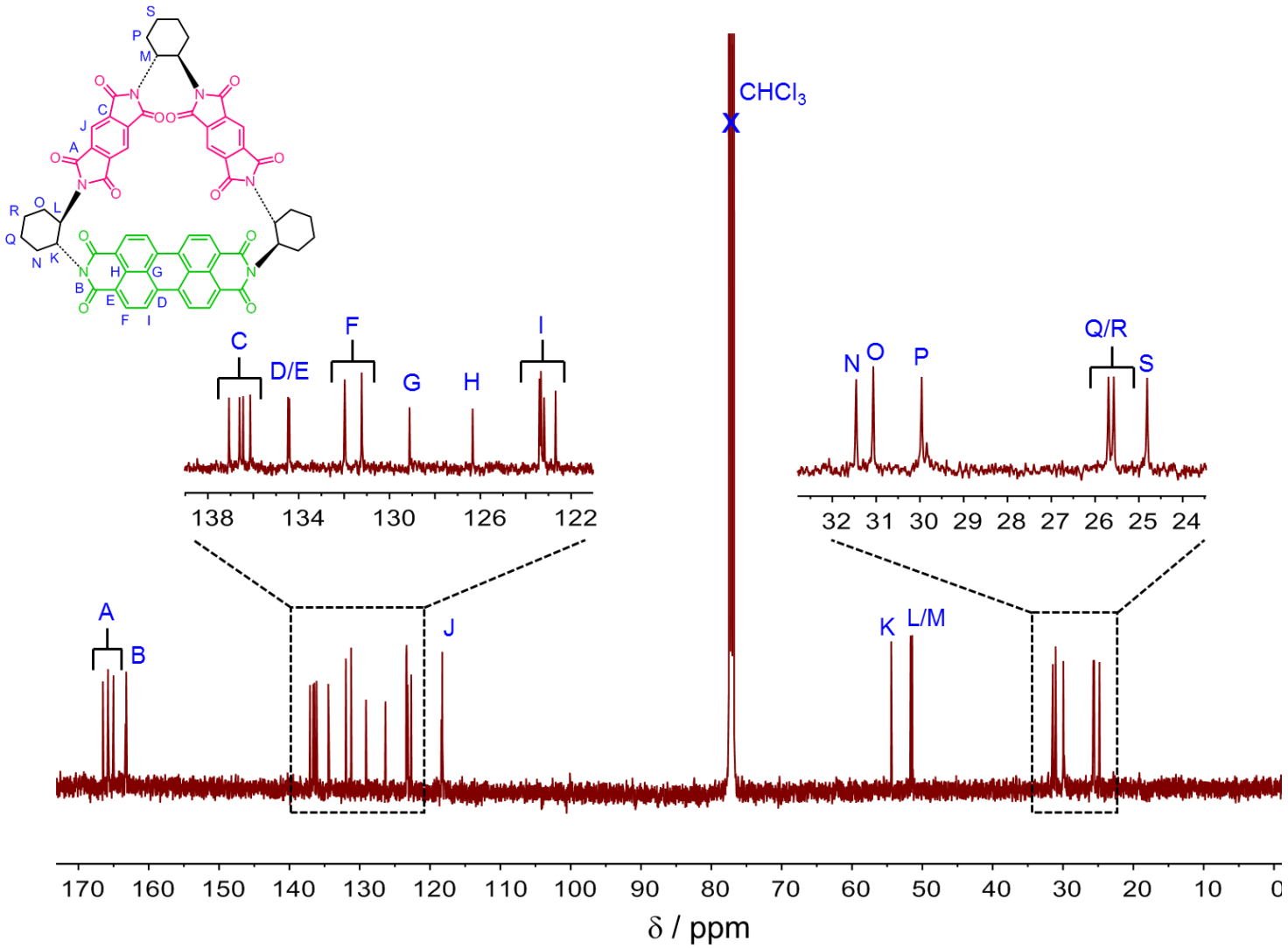

Figure S2. Annotated ^{13}C NMR spectrum (125 MHz, $CDCl_3$, 298 K) of **(−)-2PMDI-1PDI-Δ**.

c) ^{1}H NMR Spectrum of (−)-2NDI-1PDI-Δ in $CDCl_3$:

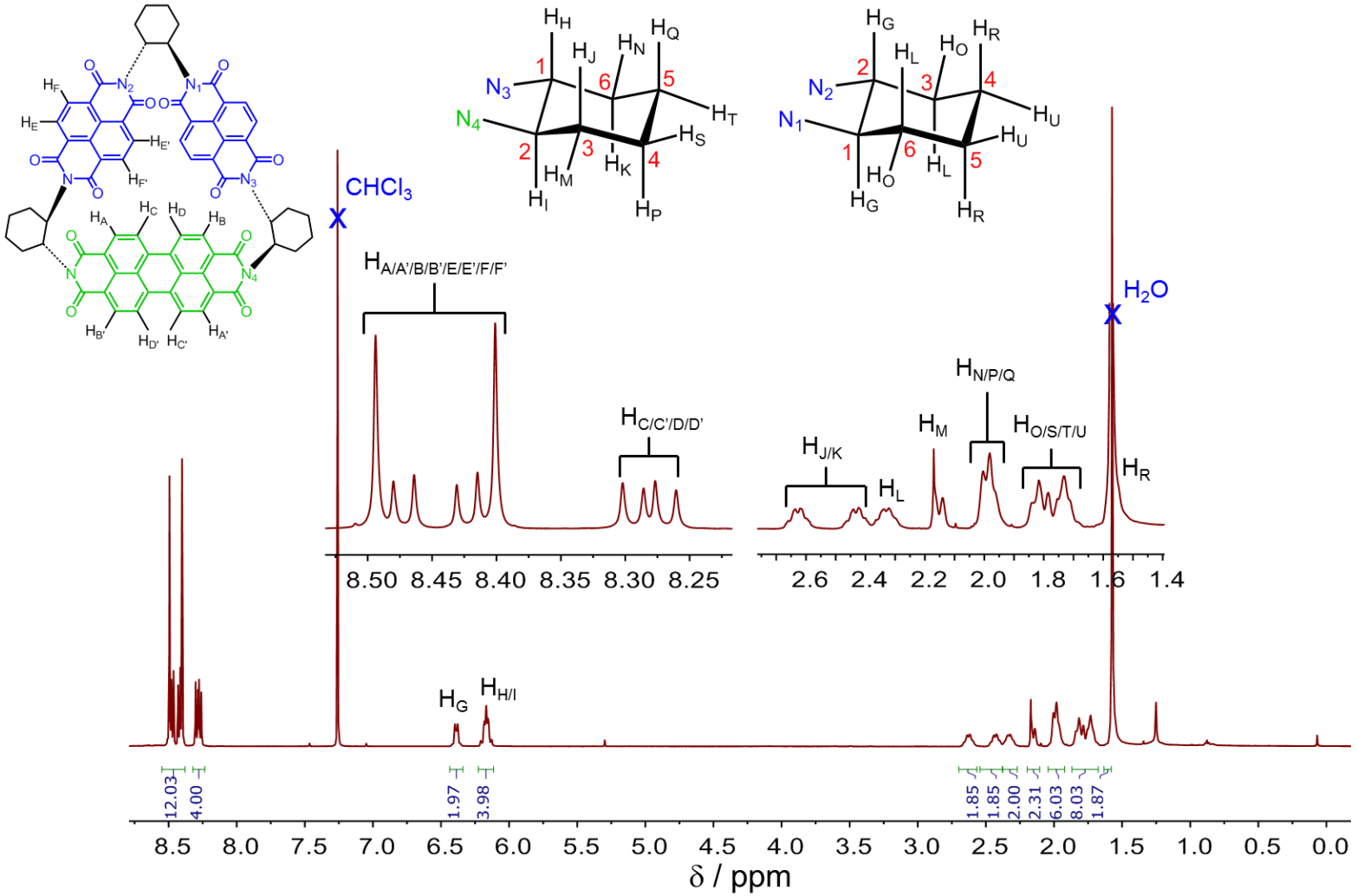

Figure S3. Annotated ^{1}H NMR spectrum (500 MHz, $CDCl_3$, 298 K) of **(−)-2NDI-1PDI-Δ**.

d) ^{13}C NMR Spectrum of **(−)-2NDI-1PDI-Δ in $CDCl_3$:**

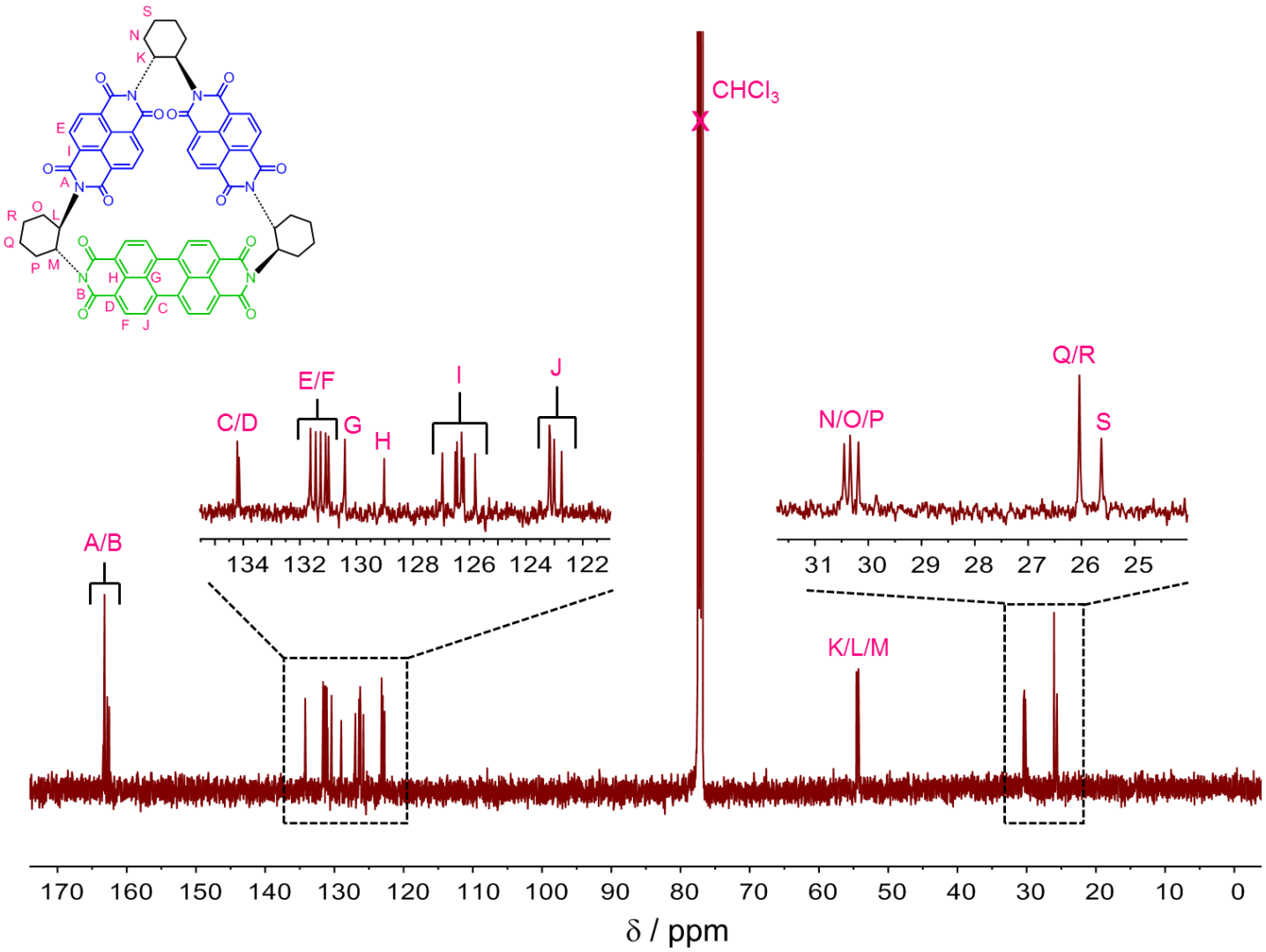

Figure S4. Annotated ^{13}C NMR spectrum (125 MHz, $CDCl_3$, 298 K) of **(−)-2NDI-1PDI-Δ**.

e) A comparison of ^{13}C NMR spectra of all triangular macrocycles:

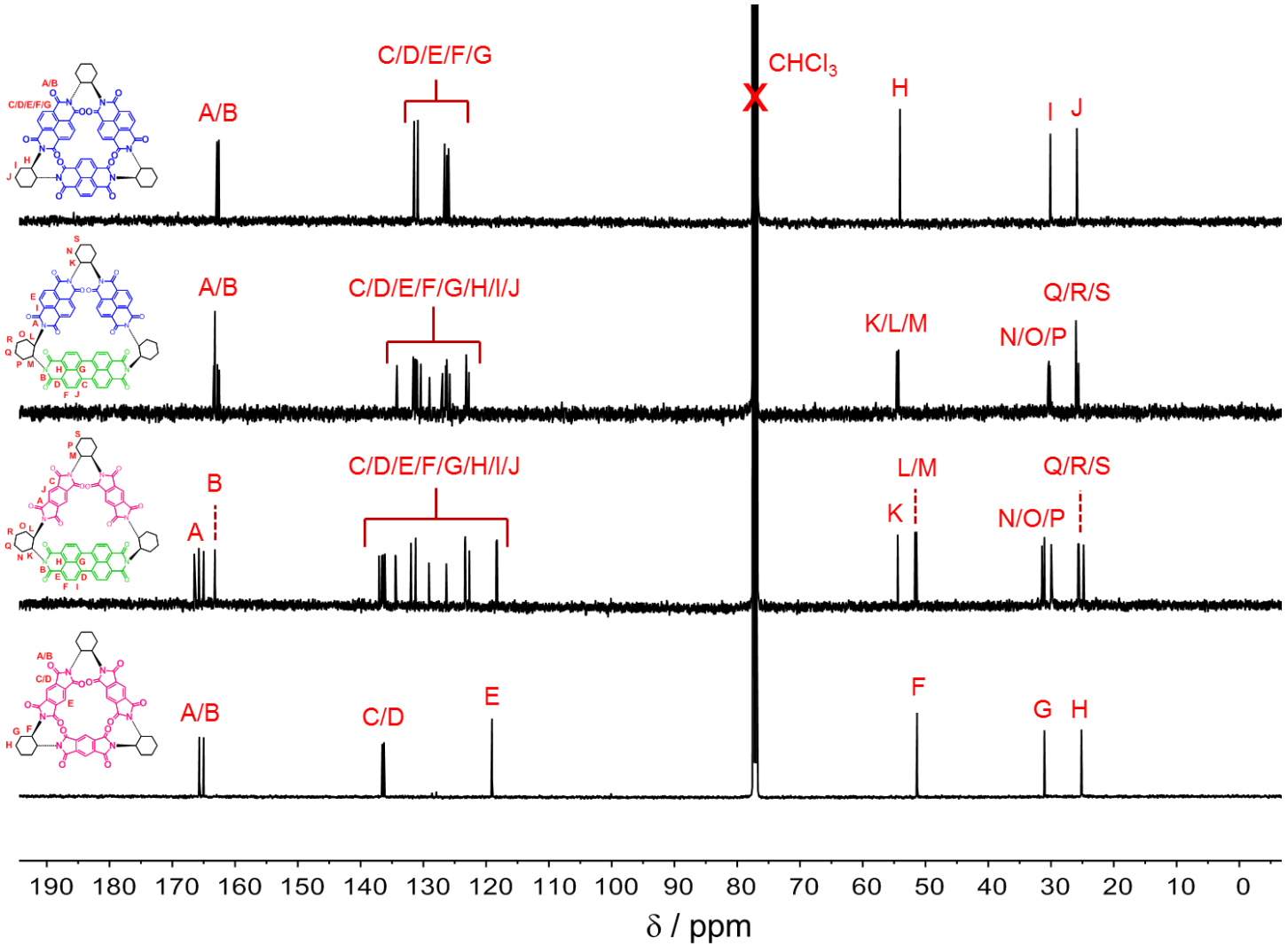

Figure S5. Comparison of the annotated ^{13}C NMR spectra (125 MHz, $CDCl_3$, 298 K) of the molecular triangles **(−)-3NDI-Δ, (−)-2NDI-1PDI-Δ, (−)-2PMDI-1PDI-Δ** and **(−)-3PMDI-Δ**.

f) Variable-temperature ^{1}H NMR Spectrum of (−)-2PMDI-1PDI-Δ in CD_3SOCD_3:

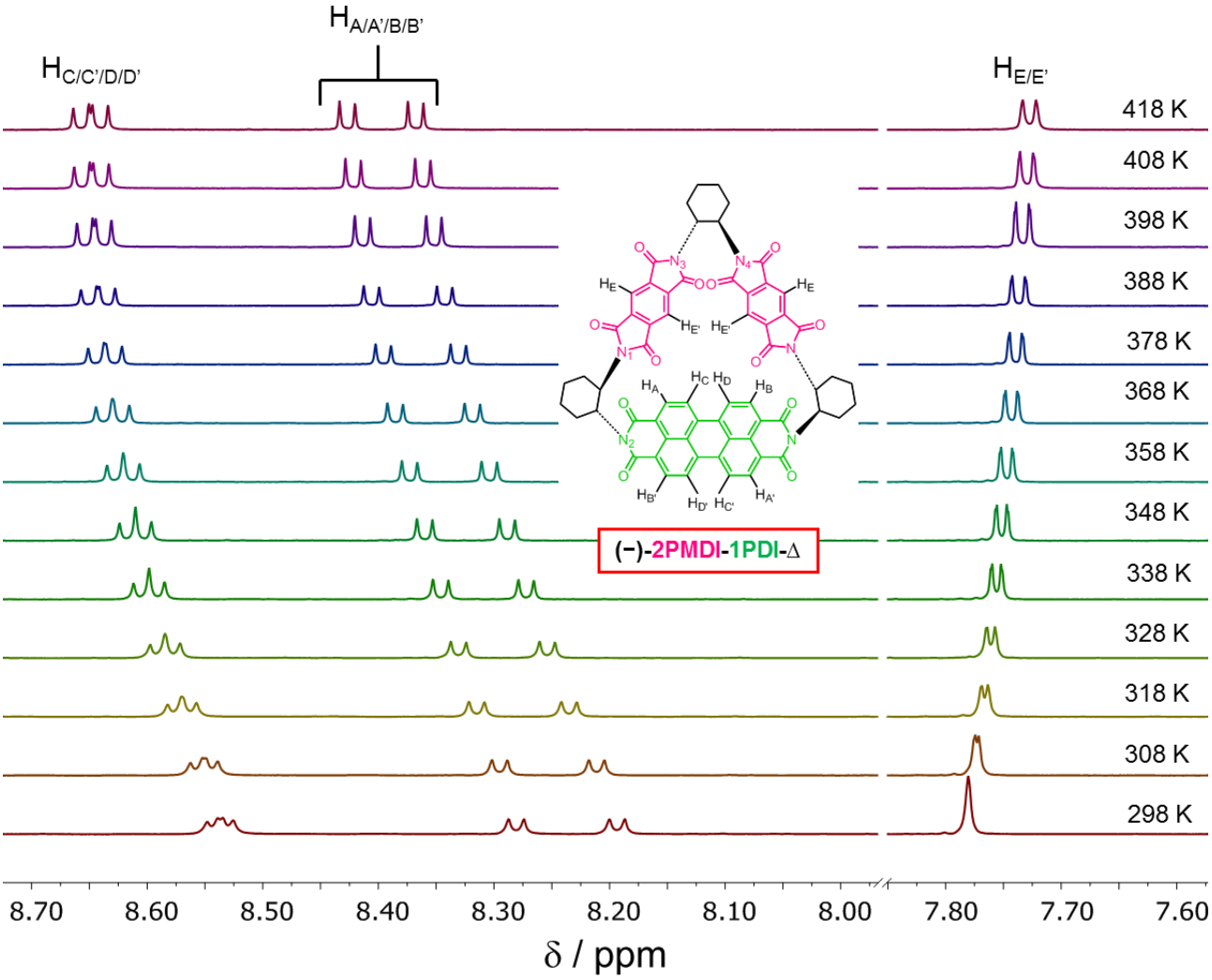

Figure S6. Variable-temperature ^{1}H NMR spectra (600 MHz, CD_3SOCD_3) in the aromatic region of the isosceles triangle **(−)-2PMDI-1PDI-Δ**. It should be noted that the downfield shift of the resonances for the PDI protons ($H_{A/A'/B/B'/C/C'/D/D'}$) of **(−)-2PMDI-1PDI-Δ** can be attributed to the weakening of the intermolecular PDI-PDI π-dimers upon increasing the temperature at the investigated concentration of about 3 mM. However, the upfield shift of the resonances observed for the PMDI protons ($H_{E/E'}$) **(−)-2PMDI-1PDI-Δ** is consistent with our previous observations[4] for **(−)-2PMDI-1NDI-Δ**.

g) Variable-temperature ^{1}H NMR Spectrum of **(−)-2NDI-1PDI-Δ in CD_3SOCD_3:**

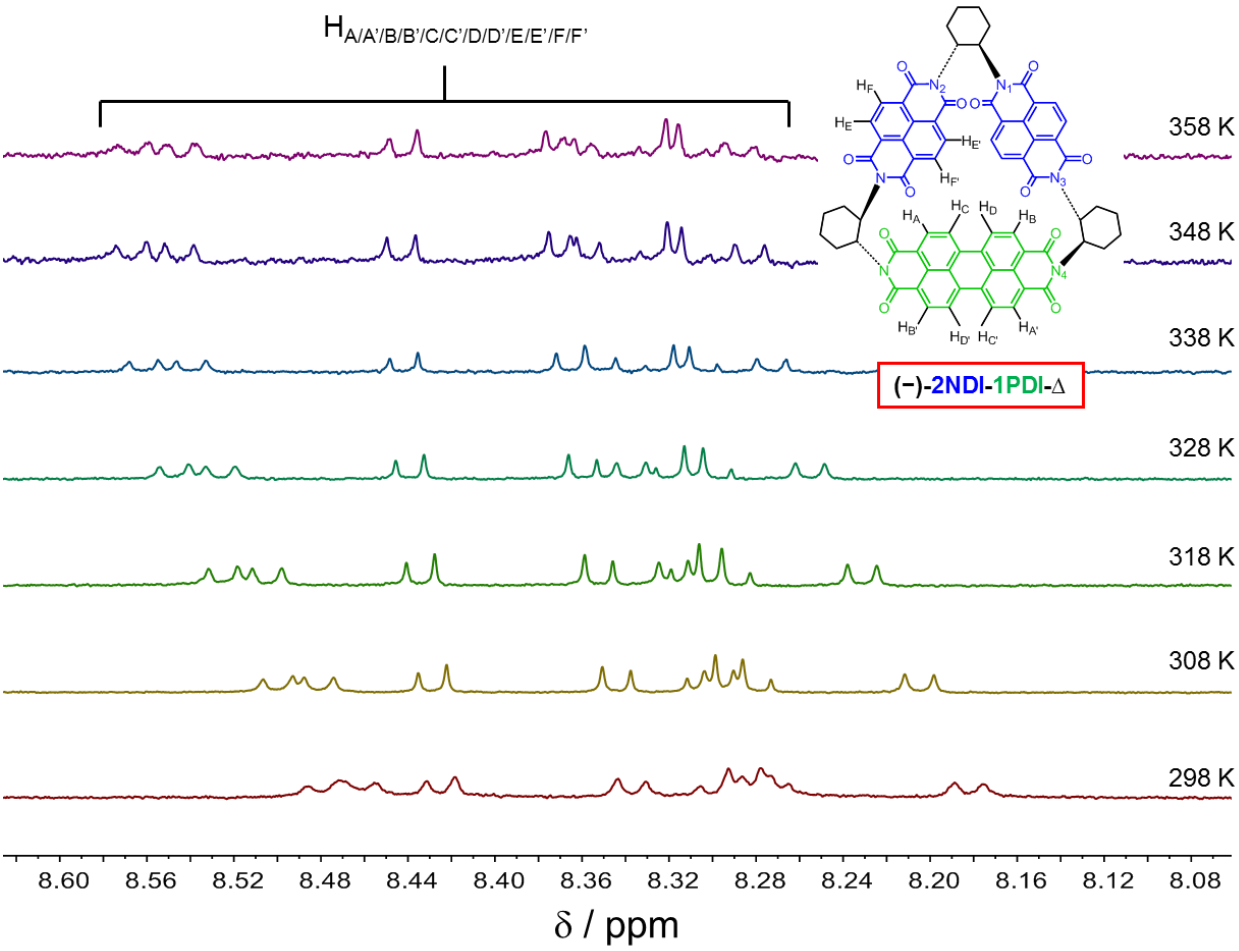

Figure S7. Variable-temperature ^{1}H NMR spectra (600 MHz, CD_3SOCD_3) in the aromatic region of the isosceles triangle **(−)-2NDI-1PDI-Δ**. It should be noted that the downfield shift of the resonances for the aromatic protons of **(−)-2NDI-1PDI-Δ** can be attributed to the weakening of the intermolecular PDI-PDI π-dimers upon increasing the temperature. Nonetheless, the accurate concentration of the sample could not be measured because of the poor solubility of **(−)-2NDI-1PDI-Δ**, relative to that of **(−)-2PMDI-1PDI-Δ**, in CD_3SOCD_3 which resulted in precipitation during the course of the experiment.

Section D. Quantum mechanical (QM) calculations

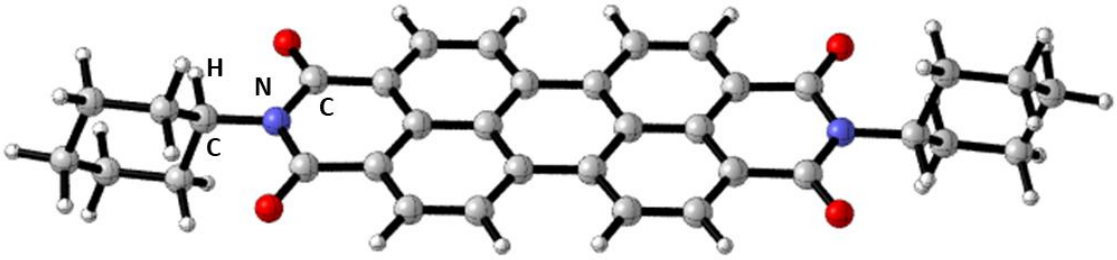

Figure S8. Graphical representation of **Ref-PDI**, calculated on the level of M06-2X density functional with 6-311G(d,p) basis sets, showing the dihedral rotation of ∠H–C–N–C.

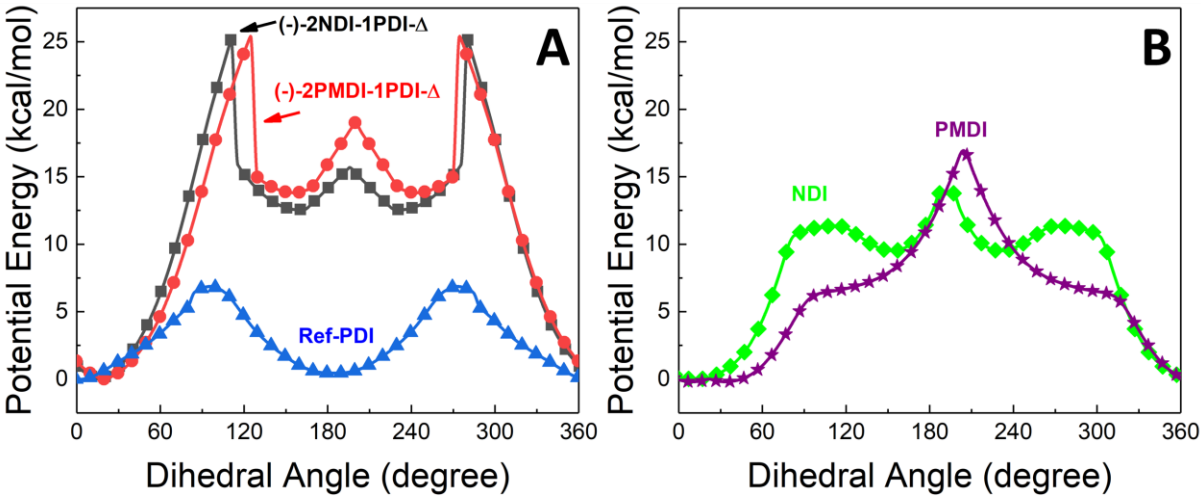

Figure S9. (A) Potential energy surface as a function of the dihedral angle (∠H–C–N–C) for PDI subunits present in **Ref-PDI** (in blue), **(−)-2PMDI-1PDI-Δ** (in red) and **(−)-2NDI-1PDI-Δ** (in black); (B) NDI subunit in **(−)-2NDI-1PDI-Δ** (in green) and PMDI subunit in **(−)-2PMDI-1PDI-Δ** (in purple).

Section E. Variable-Temperature Powder XRD (VT-PXRD)

Powder X-ray diffractions were conducted on a STOE-STADI MP powder diffractometer equipped with an asymmetric curved Germanium monochromator (CuKα1 radiation, λ = 1.54056 Å) and one-dimension silicon strip detector (MYTHEN2 1K from DECTRIS). The line focused Cu X-ray tube was operated at 40 kV and 40 mA. Samples for structural analysis were measured at room temperature in transmission geometry. The VT-PXRD experiments of both the as-synthesized isosceles triangles were conducted in a spinning capillary tube with the temperature varying from 298 up to 473 K under air. The samples were then cooled to room temperature.

a) VT-PXRD of the powder sample of **(−)-2PMDI-1PDI-Δ**:

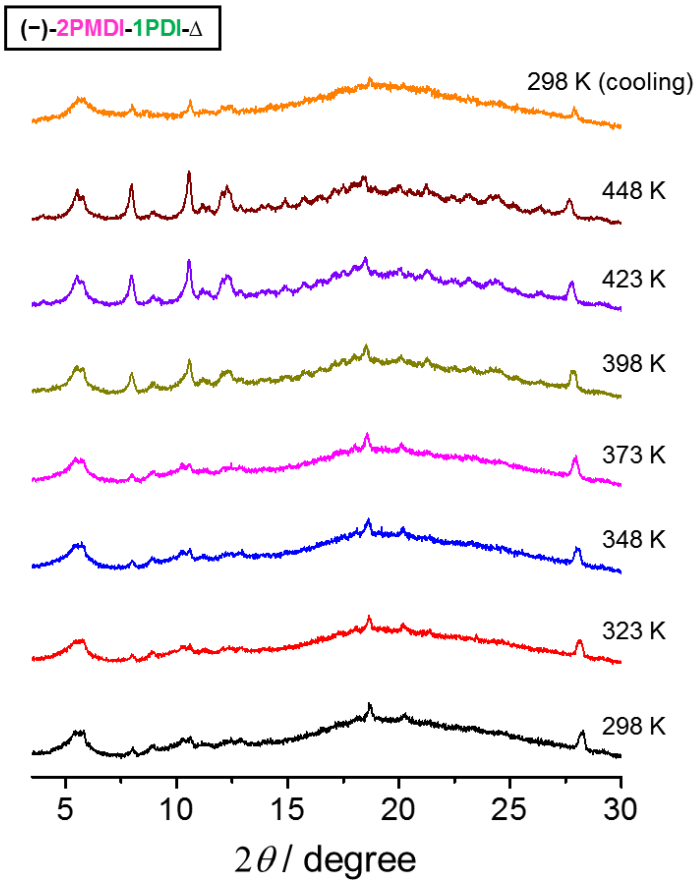

Figure S10. Variable-temperature PXRD patterns of the as-synthesized powder sample of **(−)-2PMDI-1PDI-Δ**. The patterns indeed suggest that **(−)-2PMDI-1PDI-Δ** is semi-crystalline as evidenced by the relatively broad peaks at 298 K which gradually sharpen upon increasing the temperature above 373 K (b.p. of H_2O), while it retained the same degree of crystallinity upon subsequent cooling to room temperature.

b) VT-PXRD of the powder sample of **(−)-2NDI-1PDI-Δ**:

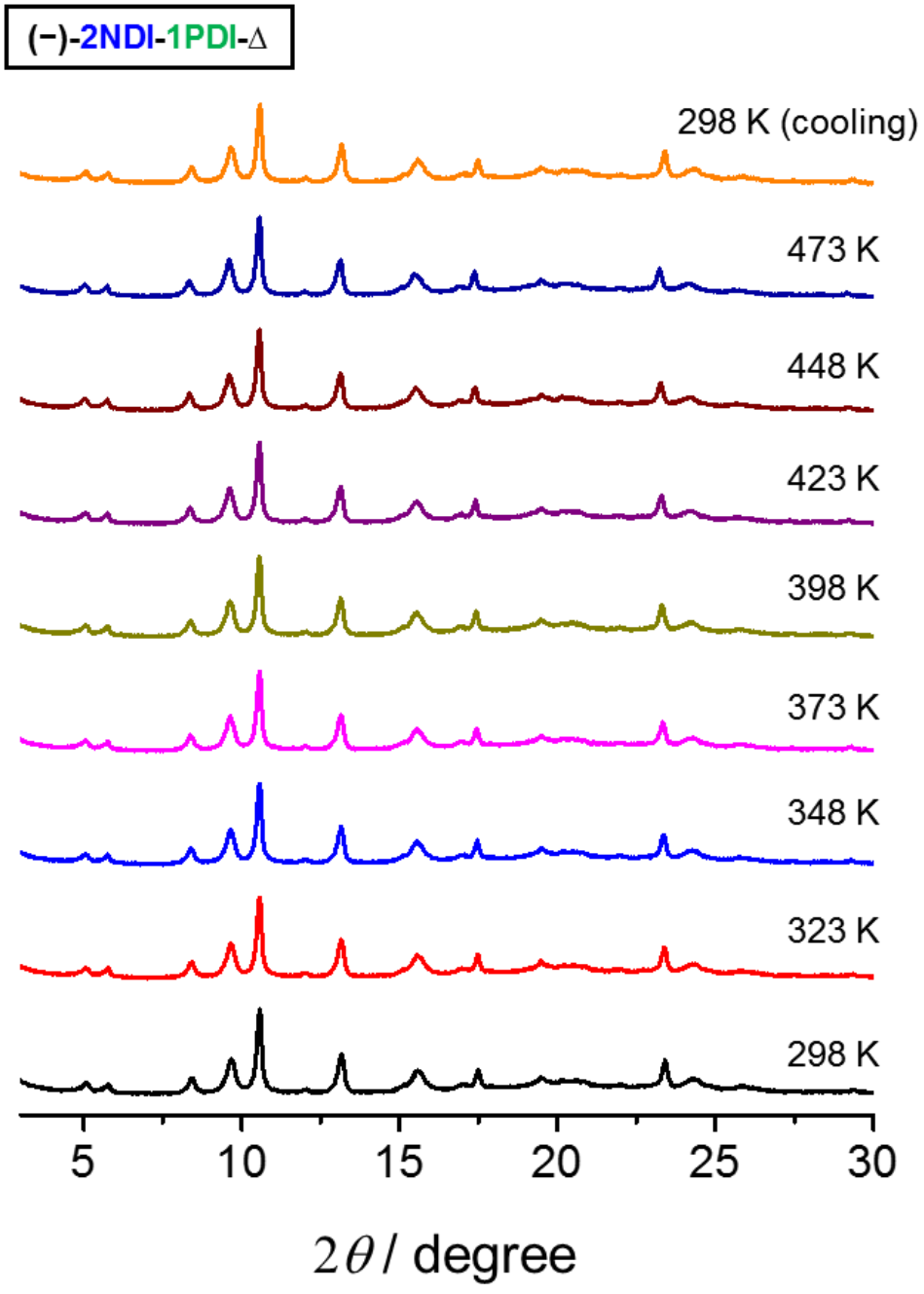

Figure S11. Variable-temperature PXRD patterns of the as-synthesized powder sample of **(−)-2NDI-1PDI-Δ**. The patterns indeed suggest that the crystalline structure is thermally stable up to 473 K which retains the same degree of crystallinity after subsequent cooling to room temperature.

Section F. Thermogravimetric analysis (TGA) and circular dichroism (CD) spectroscopy

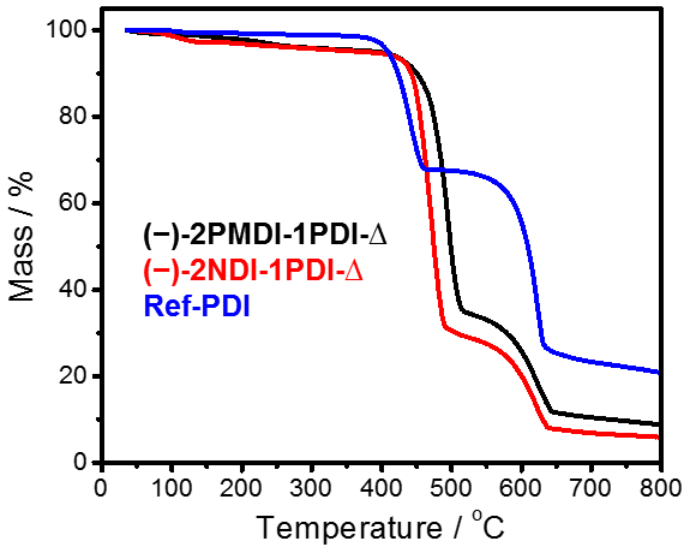

Figure S12. Thermogravimetric analyses (TGA) of the rigid isosceles triangles **(−)-2PMDI-1PDI-Δ** and **(−)-2NDI-1PDI-Δ**, and the monomeric reference compound **Ref-PDI** under a nitrogen atmosphere.

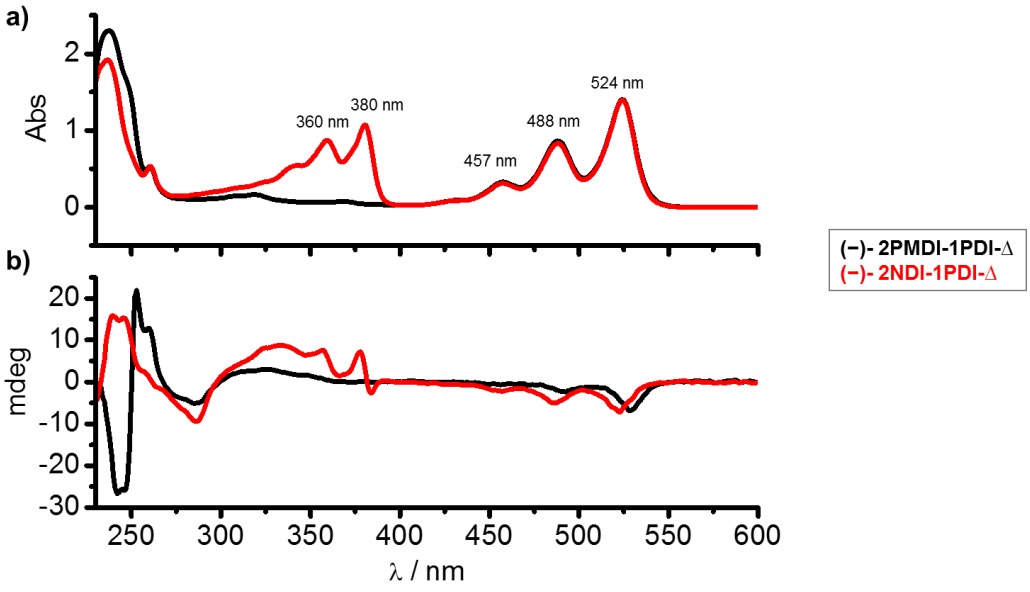

Figure S13. a) UV/Vis absorption and b) CD spectra of the rigid isosceles triangles **(−)-2PMDI-1PDI-Δ** (black traces) and **(−)-2NDI-1PDI-Δ** (red traces) recorded in CH_2Cl_2 at 298 K.

Section G. Crystallographic characterization

1) (−)-2PMDI-1PDI-Δ in 1,2-dichloroethane / *n*-hexane system (CCDC 1815897):

a) Method: Single crystals of **(−)-2PMDI-1PDI-Δ** were grown by slow vapor diffusion of *n*-hexane into a 3.0 mM solution in 1,2-dichloroethane over the course of 3 days. A suitable single crystal was selected and the crystal was mounted on a MITIGEN holder in Paratone oil on a Kappa Apex 2 diffractometer. The crystal was kept at 99.99 K during data collection. Using Olex2,[15] the structure was solved with the ShelXT[16] structure solution program using Direct Methods and refined with the ShelXL[17] refinement package using Least Squares minimization.

b) Crystal data: Empirical formula = $C_{131.3}H_{100.6}Cl_{1.3}N_{12}O_{24}$, formula weight = 2276.52, crystal system = orthorhombic, space group = $P2_12_12$ (no. 18), a = 30.1044(9), b = 31.9984(10), c = 12.4179(4) Å, α = β = γ= 90°, V = 11962.1(6) Å^3, Z = 4, T = 99.99 K, μ(CuKα) = 0.982 mm^{-1}, D_{calc} = 1.264 g/mm^3, 86166 reflections measured (5.872 ≤ 2Θ ≤ 136.662), 21606 unique (R_{int} = 0.0722, R_{sigma} = 0.0555) which were used in all calculations. The final R_1 was 0.0611 (I > 2σ(I)) and wR_2 was 0.1685 (all data).

c) Refinement details: The enhanced rigid-bond restraint (SHELX keyword RIGU) was applied on the *n*-hexane solvent.[18] Distance restraints were imposed on the C-Cl bonds on the dichloroethane solvent molecule to be similar. The dichloroethane occupancy was allowed to be refined. Rigid bond restraints (esd 0.01) were imposed on the displacement parameters of the dichloroethane solvent molecule.

d) Solvent treatment details: Total solvent accessible volume / cell = 1593.5 Å^3 [13.3%] Total electron count / cell = 437.4. The solvent masking procedure as implemented in Olex2 was used to remove the electronic contribution of solvent molecules from the refinement. As the exact solvent content is not known, only the atoms used in the refinement model are reported in the formula here.

***2)* (−)-2NDI-1PDI-Δ in $CHCl_3$ (CCDC 1815898):**

a) Method: Single crystals of **(−)-2NDI-1PDI-Δ** were grown by slow evaporation of 6 mM solution in $CHCl_3$ over the course of 7 days. A suitable single crystal was selected and the crystal was mounted on a MITIGEN holder in Paratone oil on a Kappa Apex 2 diffractometer. The crystal was kept at 99.99 K during data collection. Using Olex2[15], the structure was solved with the ShelXT[16] structure solution program using Intrinsic Phasing and refined with the XL[19] refinement package using Least Squares minimization.

b) Crystal data: Empirical formula = $C_{145}H_{97}Cl_{15}N_{12}O_{24}$, formula weight= 2923.09, monoclinic, space group *C*2 (no. 5), a = 43.1347(12), b = 14.6175(4), c = 24.2886(6) Å, α = 90°, β = 102.9369(16)°, γ = 90°, V = 14925.8(7) Å^3, Z = 4, T = 99.99 K, μ(CuKα) = 3.111 mm^{-1}, D_{calc} = 1.301 g/mm^3, 57433 reflections measured ($3.732 \leq 2\Theta \leq 127.504$), 24109 unique ($R_{int}$ = 0.0874, R_{sigma} = 0.1027) which were used in all calculations. The final R_1 was 0.0634 ($I > 2\sigma(I)$) and wR_2 was 0.1753 (all data).

c) Refinement details: The enhanced rigid-bond restraint (SHELX keyword RIGU) was applied globally.[18]

d) Solvent treatment details. The solvent masking procedure as implemented in Olex2 was used to remove the electronic contribution of solvent molecules from the refinement. As the exact solvent content is not known, only the atoms used in the refinement model are reported in the formula here. Total solvent accessible volume / cell = 3130.9 Å^3 [21.0%] Total electron count / cell = 958.5.

***3)* (−)-2PMDI-1PDI-Δ in $CHCl_3$ / *n*-hexane system (CCDC 1879108):**

a) Method: Single crystals of **(−)-2PMDI-1PDI-Δ** were grown by slow vapor diffusion of *n*-hexane into a 3.0 mM solution in $CHCl_3$ over the course of 3 days. A suitable crystal was selected and the crystal was mounted on a MITIGEN holder in Paratone oil on a Kappa Apex 2 diffractometer. The crystal was kept at 99.99 K during data collection. Using Olex2,[15] the structure was solved with the ShelXS[19] structure solution program using Direct Methods and refined with the XL[19] refinement package using Least Squares minimization.

b) Crystal Data: Empirical Formula = $C_{125}H_{85}Cl_3N_{12}O_{24}$, formula weight = 2245.40, crystal system = orthorhombic, space group = $P2_12_12$ (no. 18), a = 30.418(3) Å, b = 31.784(3) Å, c = 12.380(12) Å, α = β = γ= 90°, V = 11969(2) Å^3, Z = 4, T = 99.99 K, μ(CuKα) = 1.316 mm^{-1}, D_{calc} = 1.246 g/mm^3, 199950 reflections measured ($4.02 \leq 2\Theta \leq 137.344$), 21787 unique ($R_{int}$ = 0.0826, R_{sigma} = 0.0492) which were used in all calculations. The final R_1 was 0.0578 ($I > 2\sigma(I)$) and wR_2 was 0.1756 (all data).

c) Refinement Details*:* No special refinement necessary.

***d*) Solvent Treatment Details:** The solvent masking procedure as implemented in Olex2 was used to remove the electronic contribution of solvent molecules from the refinement. As the exact solvent content is not known, only the atoms used in the refinement model are reported in the formula here. Total solvent accessible volume / cell = 2565.3 Å^3 [21.3%] Total electron count / cell = 745.2

4) **Solvent-free crystals of (−)-2PMDI-1PDI-Δ (CCDC 1879109):**

a) Method: Solvent-free single crystals of **(−)-2PMDI-1PDI-Δ** were obtained by air drying, for several days, the single crystals grown by slow vapor diffusion of *n*-hexane into a 3.0 mM solution in $CHCl_3$. A suitable crystal was selected and the crystal was mounted on a MITIGEN holder in Paratone oil on a Bruker Kappa APEX CCD area detector diffractometer. The crystal was kept at 99.99 K during data collection. Using Olex2,[15] the structure was solved with the ShelXS[19] structure solution program using Direct Methods and refined with the ShelXL[17] refinement package using Least Squares minimization.

b) Crystal Data: Empirical Formula = $C_{62}H_{42}N_6O_{12}$, formula weight = 1063.01, crystal system = orthorhombic, space group = $P2_12_12$ (no. 18), a = 30.307(18) Å, b = 32.069(2) Å, c = 12.6054(8) Å, α = β = γ= 90°, V = 12251.5(13) Å^3, Z = 8, T = 99.99 K, μ(CuKα) = 0.672 mm^{-1}, D_{calc} = 1.153 g/mm^3, 43511 reflections measured (5.512 ≤ 2Θ ≤ 127.668), 19023 unique (R_{int} = 0.0896, R_{sigma} = 0.1606) which were used in all calculations. The final R_1 was 0.1129 (I > 2σ(I)) and wR_2 was 0.3309 (all data).

c) Refinement Details*:* No special refinement necessary.

d) Solvent Treatment Details: Not applicable.

Section H. Single-crystal X-Ray structures of the isosceles triangles

a) Single-crystal X-ray structures showing the host-guest complexation of the rigid isosceles triangles with solvent molecules

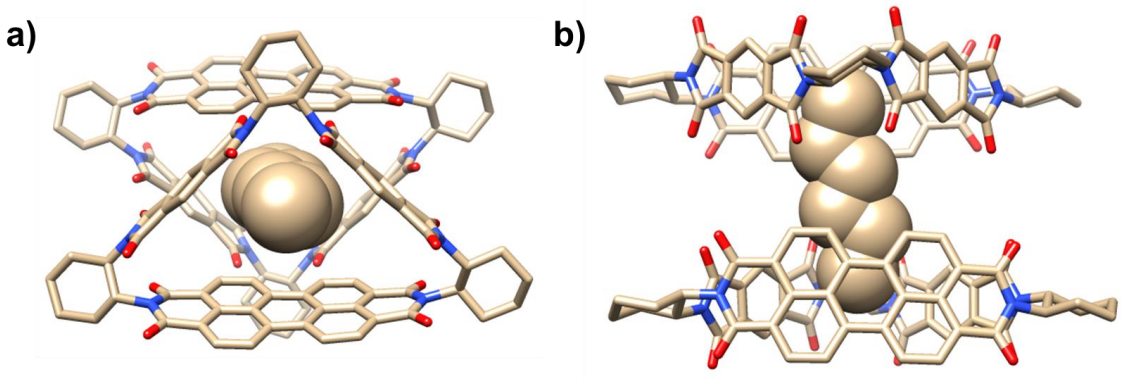

Figure S14. Single-crystal X-ray structure of (−)-2PMDI-1PDI-Δ from 1,2-dichloroethane / *n*-hexane system. (**a**) Top and (**b**) side-on views of **(−)-2PMDI-1PDI-Δ** forming a 2:1 inclusion complex with *n*–hexane molecule, depicted in space-filling representation, by means of multiple [C−H···π] interactions. H atoms are omitted for the sake of clarity.

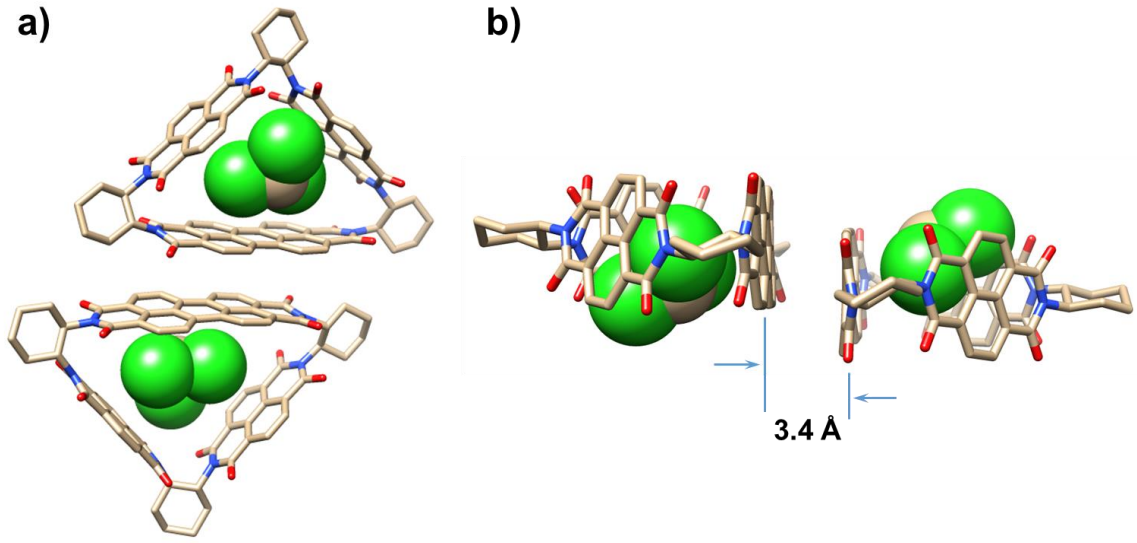

Figure S15. Single-crystal X-ray structure of (−)-2NDI-1PDI-Δ from $CHCl_3$ system. (**a**) Top and (**b**) side-on views of π−π stacking dimers of **(−)-2NDI-1PDI-Δ** where $CHCl_3$ molecules, depicted in space-filling representation, are bound to their cavities stabilized by multiple [Cl···π] interactions (~3.4 Å) with π-surfaces. H atoms are omitted for the sake of clarity.

b) Single-crystal X-ray structure of **(−)-2PMDI-1PDI-Δ** from $CHCl_3$ / *n*-hexane system.

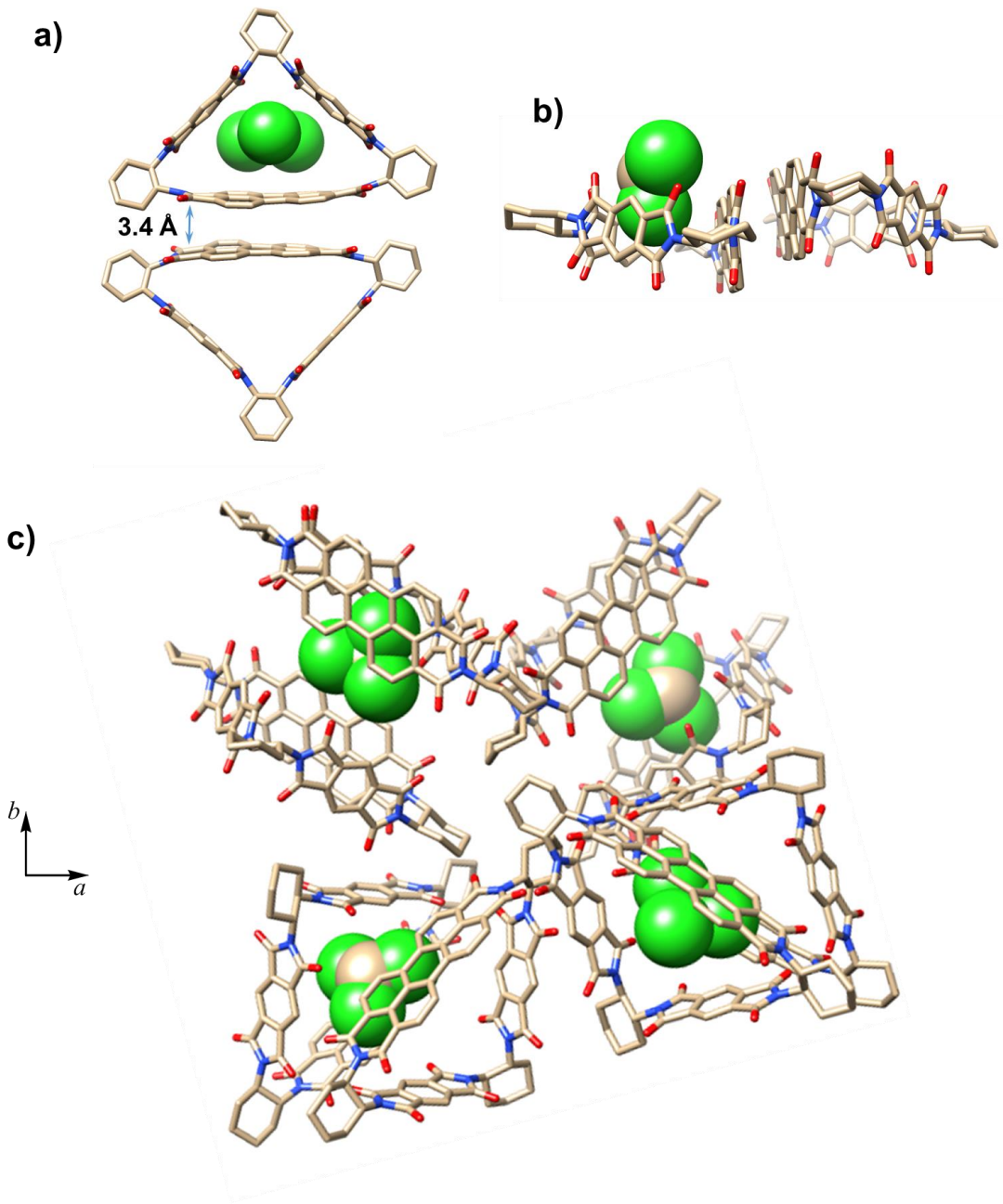

Figure S16. Single-crystal X-ray structure of (−)-2PMDI-1PDI-Δ from $CHCl_3$ / *n*-hexane system. (**a**) Plan and (**b**) side-on views of π−π stacking dimers of **(−)-2PMDI-1PDI-Δ** where $CHCl_3$ molecule, depicted in space-filling representation, is bound to one of the cavities by means of [C−H···O] interactions. **c**) A view along *c*-axis of the unit cell of **(−)-2PMDI-1PDI-Δ**. H atoms are omitted for the sake of clarity.

c) Solvent-free single-crystal X-ray structure of **(−)-2PMDI-1PDI-Δ** obtained after drying $CHCl_3$ and *n*-hexane.

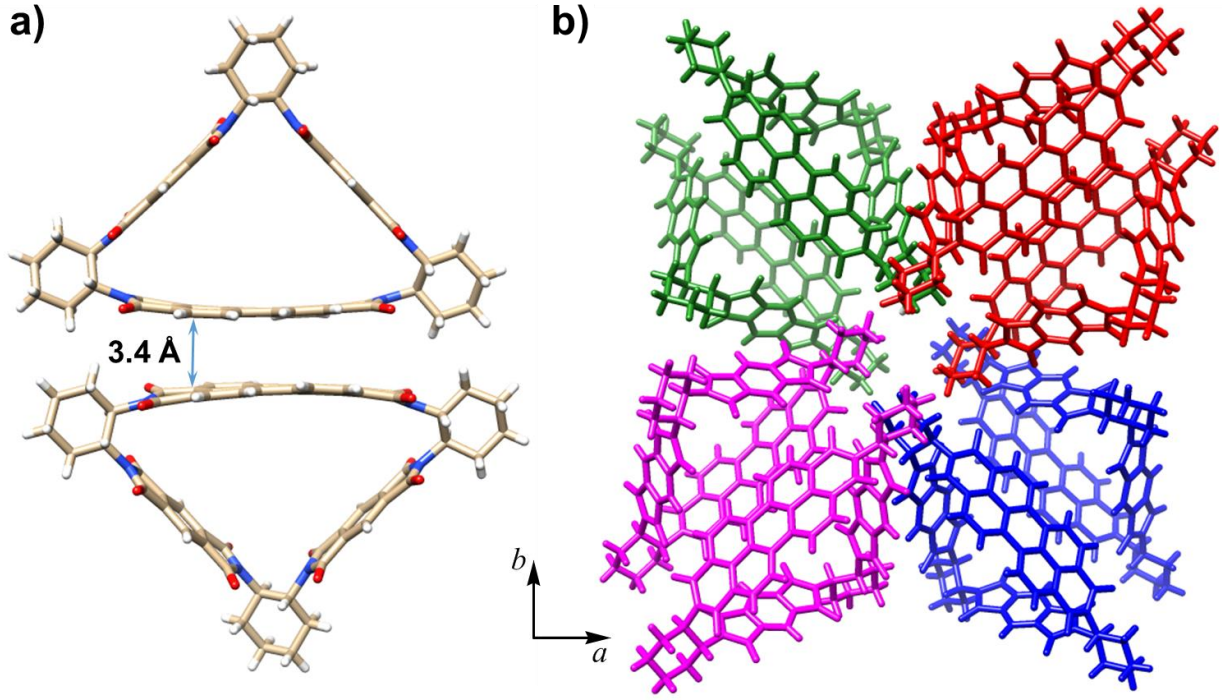

Figure S17. Solvent-free single-crystal X-ray structure of (−)-2PMDI-1PDI-Δ. (**a**) Plan view of π–π stacking (~3.4 Å) dimer of **(−)-2PMDI-1PDI-Δ**. **b**) A view along *c*-axis of the unit cell of **(−)-2PMDI-1PDI-Δ**. For the sake of clarity, in Figure **b**, four π–π dimers adopting different orientations are depicted in blue, magenta, red, and green. Note: Solvent-free single crystals of **(−)-2PMDI-1PDI-Δ** were obtained by air drying the single crystals grown by slow vapor diffusion of *n*-hexane in $CHCl_3$ solution, in order to investigate the role of solvents on the formation of discrete PDI-PDI π-dimers in the solid state. Even in solvent-free conditions, it was observed that the PDI-PDI π-dimers remained intact which exhibit similar packing arrangements and the unit cell parameters before and after removal of $CHCl_3$ from the single crystals.

Section I. Hirshfeld Surface Analyses

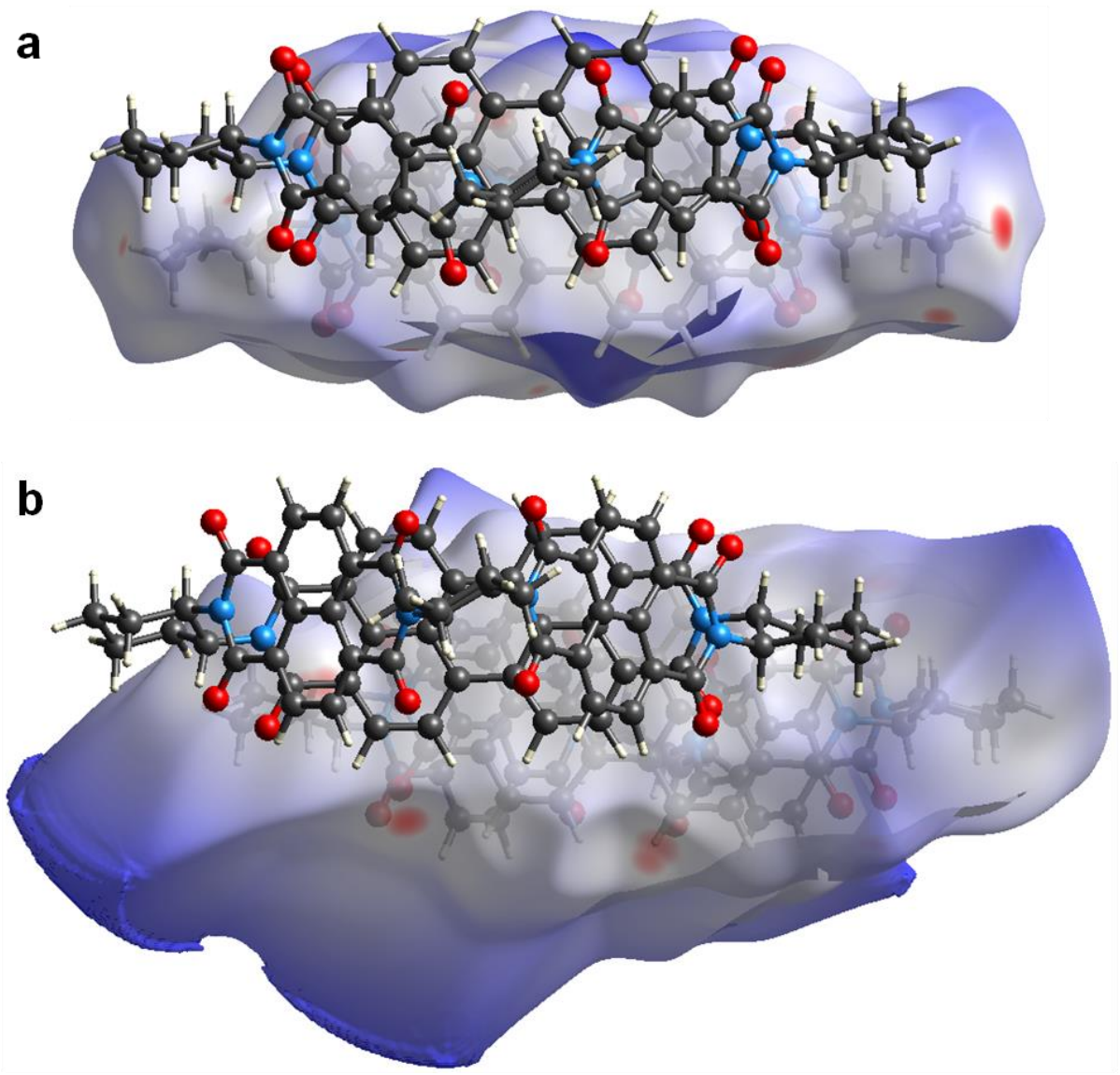

Figure S18. The Hirshfeld[20] surfaces of the π–π dimers of (**a**) **(−)-2PMDI-1PDI-Δ** and (**b**) **(−)-2NDI-1PDI-Δ** mapped with d_{norm}. The [π···π] interactions contribute 12.2% to the Hirshfeld surface of **(−)-2PMDI-1PDI-Δ** and 12.1% to the Hirshfeld surface of **(−)-2NDI-1PDI-Δ**, respectively.

Section J. Excitation-emission contour plot by fluorescence spectroscopy

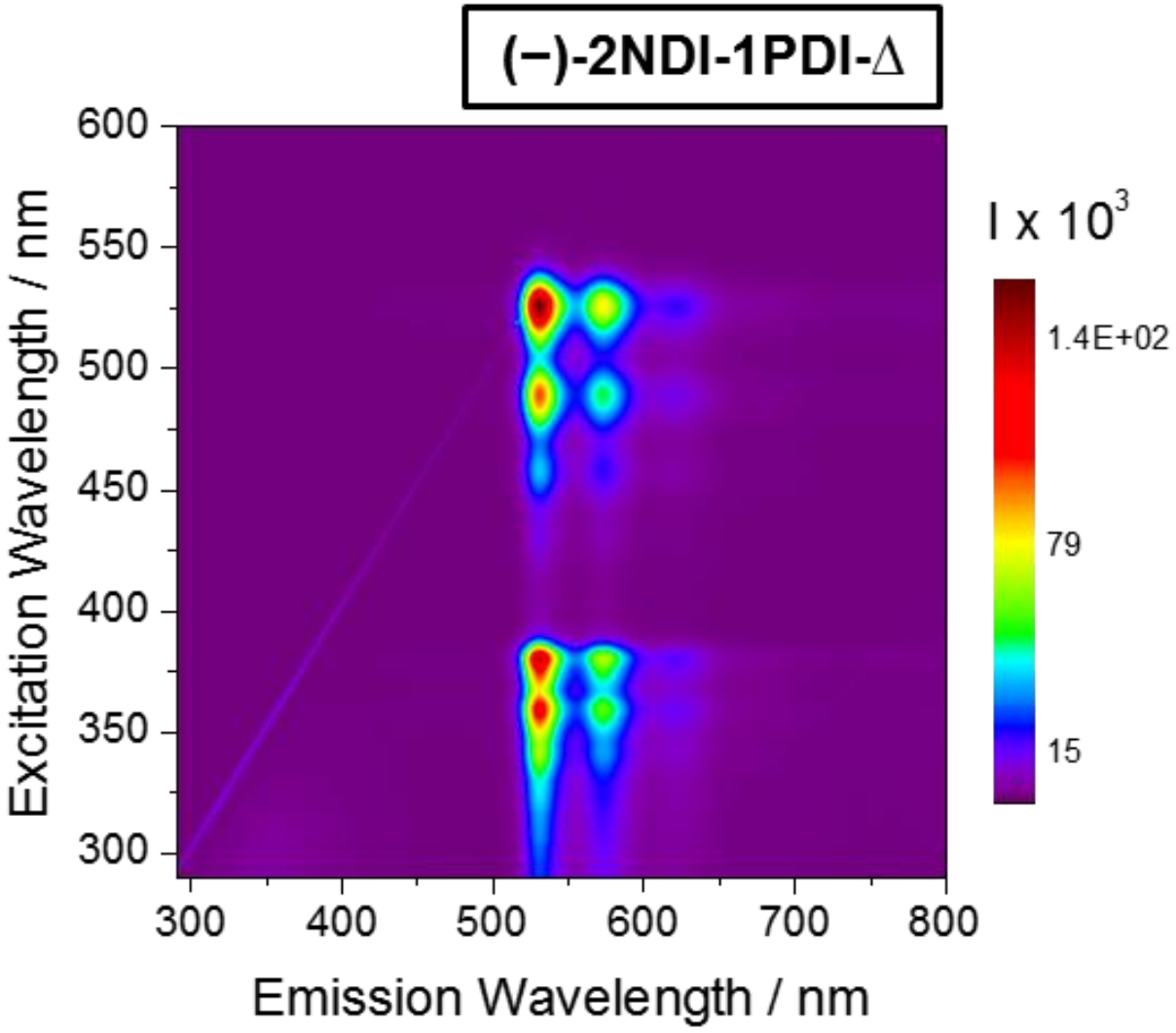

Figure S19. Excitation-emission photoluminescence contour plot for **(−)-2NDI-1PDI-Δ** recorded in CH_2Cl_2 at 298 K, suggesting the efficient energy transfer from the lowest excited singlet state of NDI to that of the PDI subunit within the isosceles triangle **(−)-2NDI-1PDI-Δ** upon photoexcitation of the NDI subunits.

Section K. Femtosecond transient absorption spectroscopy (fsTA)

a) fsTA of the monomeric reference compound **Ref-PDI** in CH_2Cl_2

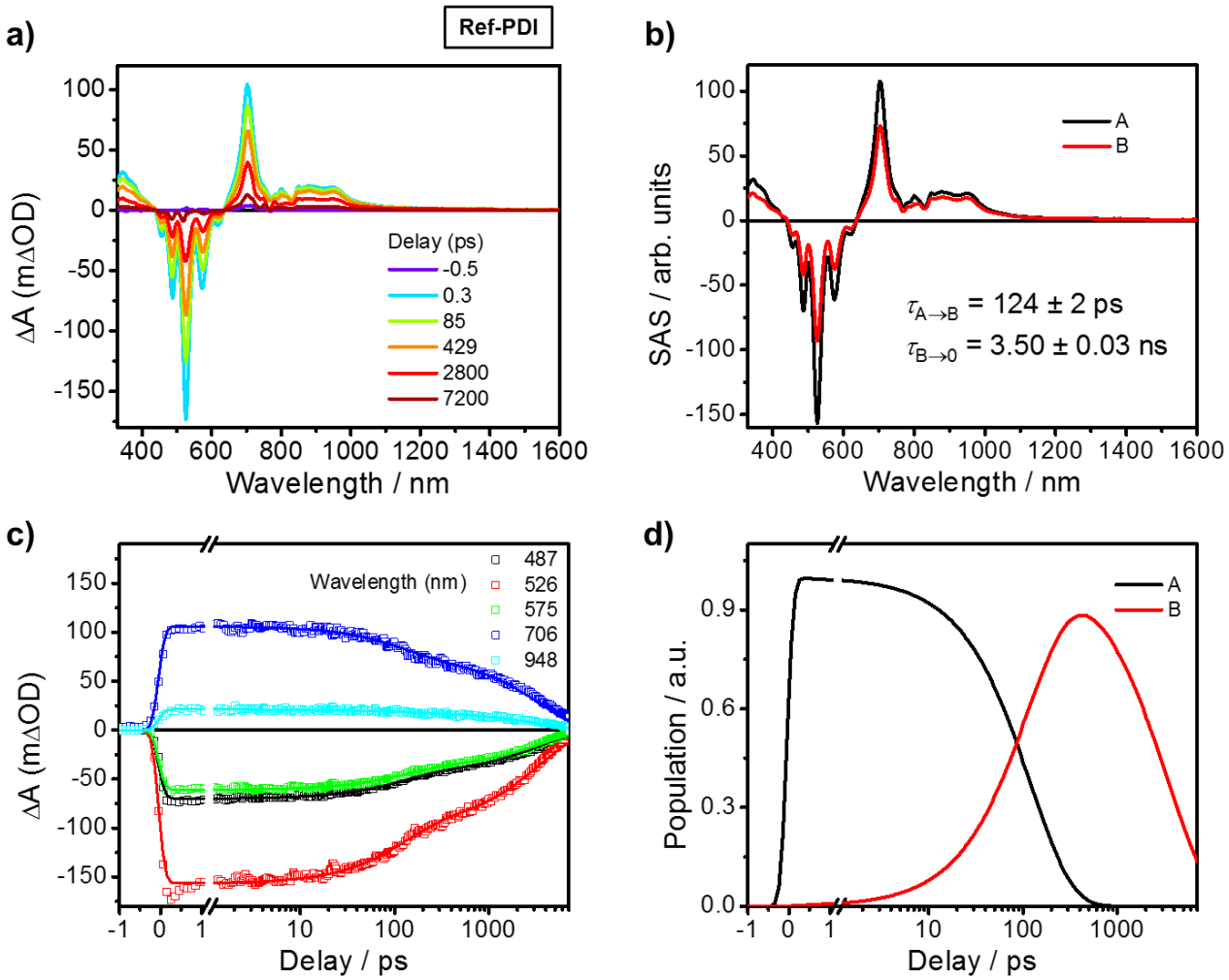

Figure S20. a) fsTA spectra and (b) species-associated spectra (SAS) and (c) multiple-wavelength fits and (d) populations of kinetic states of the monomeric reference compound **Ref-PDI** in CH_2Cl_2 upon photoexcitation at 493 nm. Different states used in this spectra are represented by A: hot S_1, B: relaxed S_1, and 0: S_0.

b) fsTA of the isosceles triangle **(−)-2PMDI-1PDI-Δ** in CH_2Cl_2

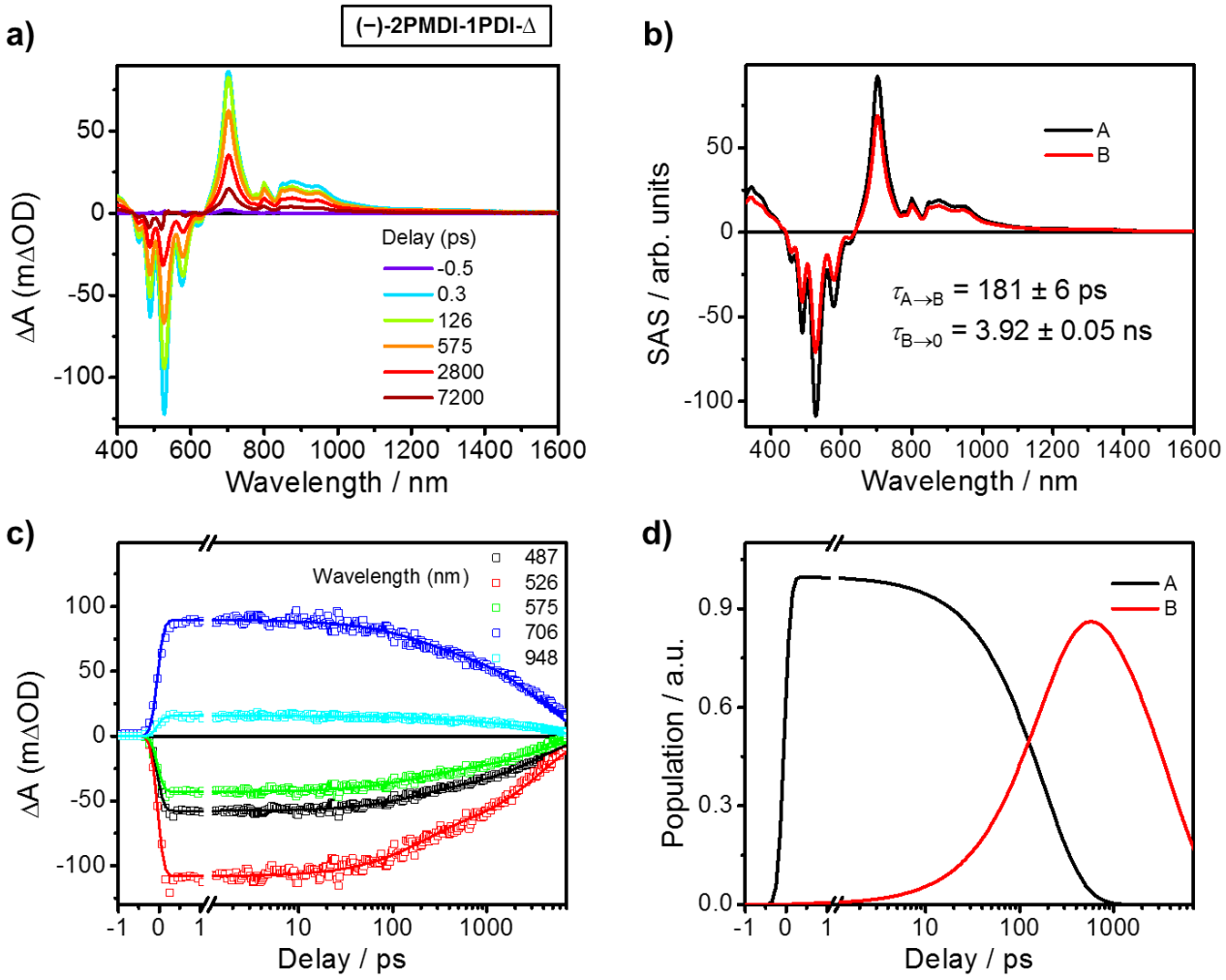

Figure S21. a) fsTA spectra and (b) species-associated spectra (SAS) and (c) multiple-wavelength fits and (d) populations of kinetic states of the monomeric reference compound **(−)-2PMDI-1PDI-Δ** in CH_2Cl_2 upon photoexcitation at 493 nm. Different states used in this spectra are represented by A: hot S_1, B: relaxed S_1, and 0: S_0.

c) fsTA of the isosceles triangle **(−)-2NDI-1PDI-Δ** in CH_2Cl_2

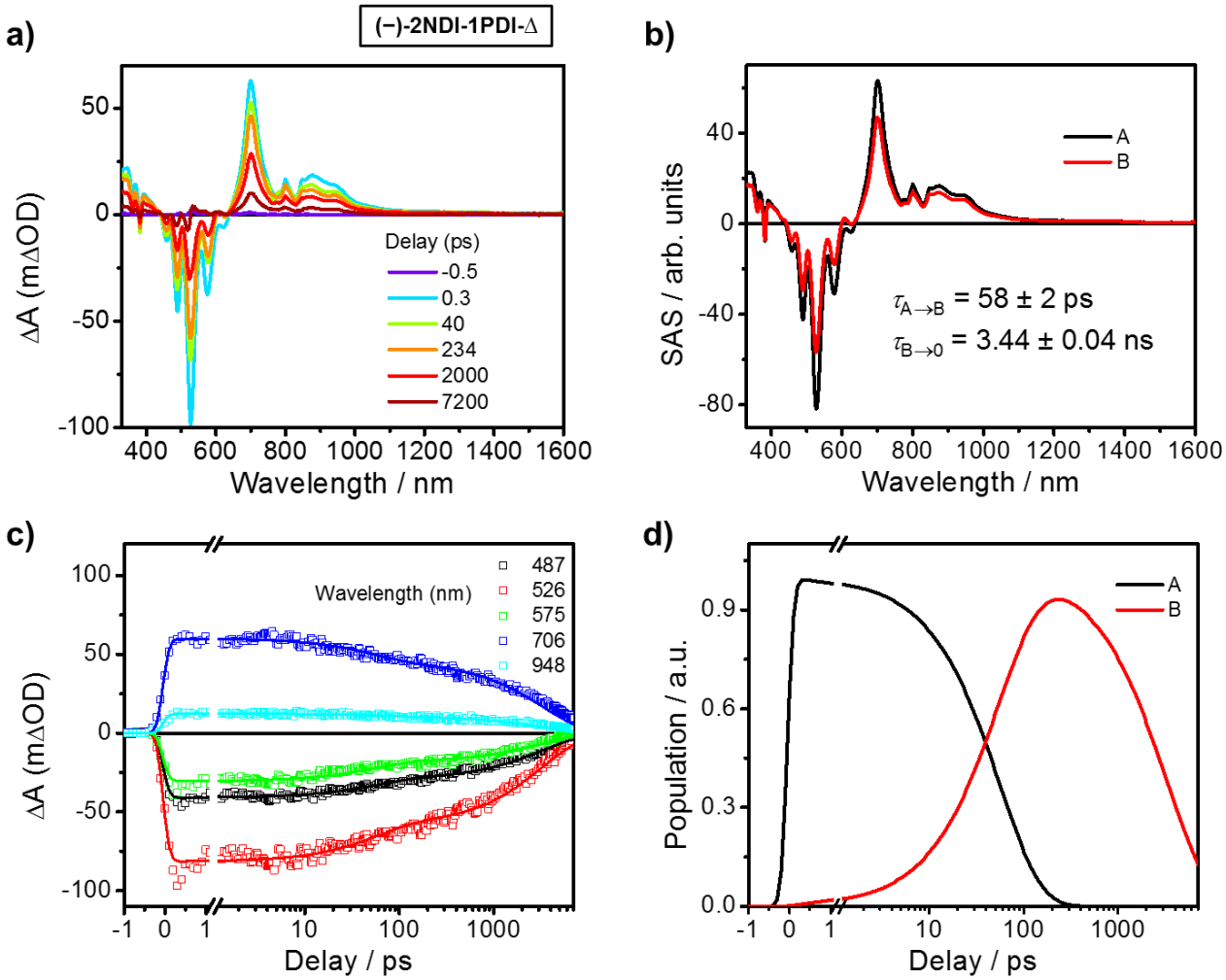

Figure S22. a) fsTA spectra and (b) species-associated spectra (SAS) and (c) multiple-wavelength fits and (d) populations of kinetic states of the monomeric reference compound **(−)-2NDI-1PDI-Δ** in CH_2Cl_2 upon photoexcitation at 493 nm. Different states used in this spectra are represented by A: hot S_1, B: relaxed S_1, and 0: S_0.

Section L. Diffuse Reflectance UV/Vis spectroscopy

The diffuse reflectance spectra of all three compounds in solid state (powder form) are shown in **Figure S17**. The linewidths of the spectral peaks corresponding to all three compounds are relatively broad with the loss of the well-resolved vibronic patterns found in solution. The observed differences in their solid state reflectance spectra are presumably a consequence of a complex combination of electronic transition dipole-dipole coupling as well as π-π overlap.

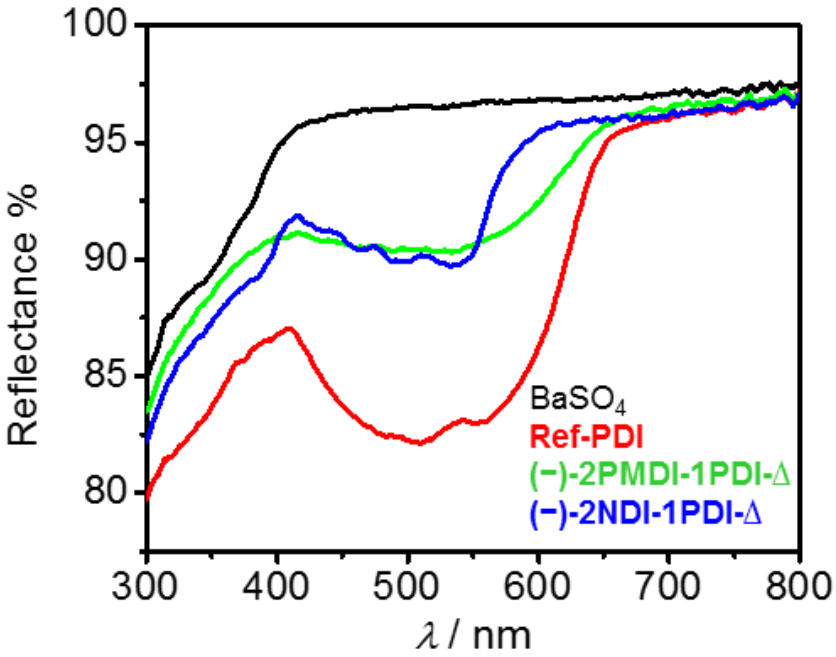

Figure S23. Diffuse Reflectance UV/Vis spectra of **Ref-PDI**, **(−)-2PMDI-1PDI-Δ** and **(−)-2NDI-1PDI-Δ** recorded for powder samples mixed with $BaSO_4$ matrix at 298 K

Section M. Photoluminescence spectroscopy in the solid state

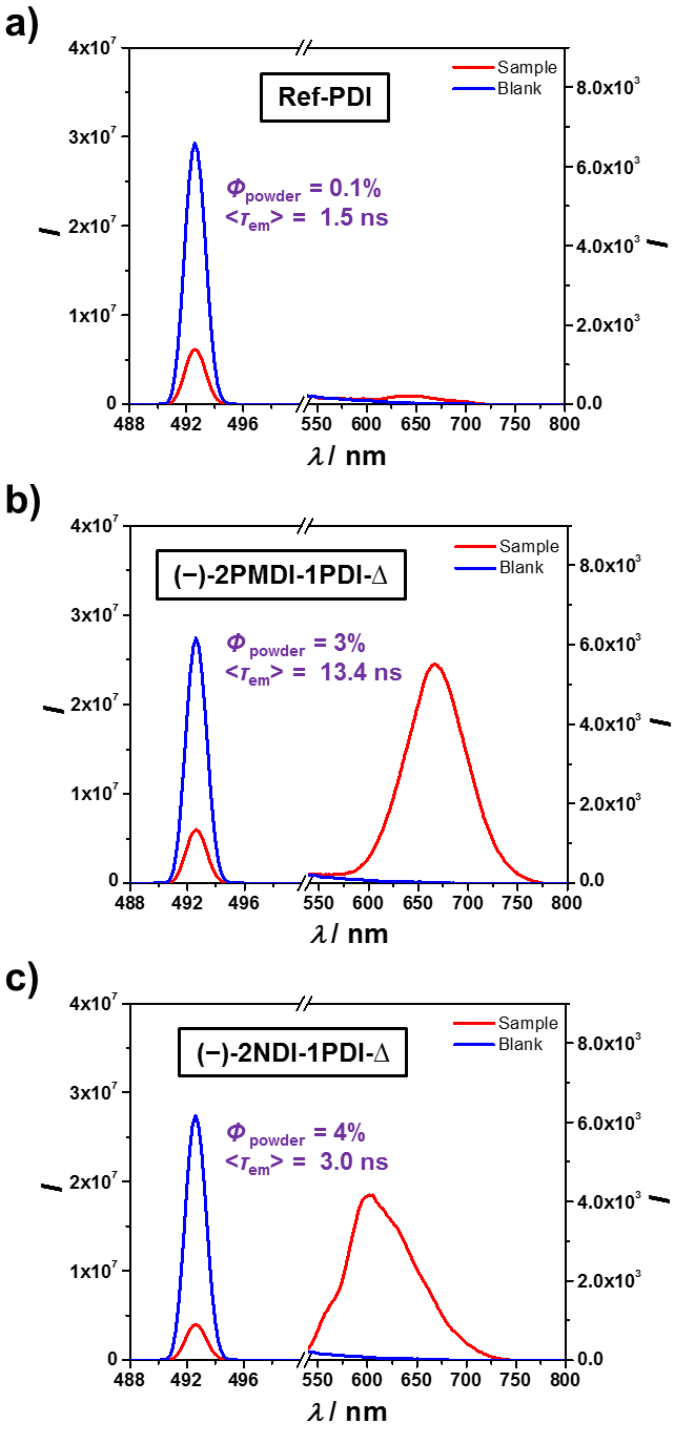

Figure S24. Traces from the photoluminescence spectra of the powder samples of (a) **Ref-PDI**, (b) **(−)-2PMDI-1PDI-Δ** and (c) **(−)-2NDI-1PDI-Δ** used for measuring the absolute photoluminescence quantum yields (Φ_{powder}) in the solid state with an integrating sphere. The fluorescence spectra of all three compounds were obtained with the excitation at 493 nm.

Section N. Thin Film X-Ray Diffraction

Thin film X-ray diffractions were conducted on a Rigaku Smartlab instrumentation configured with a high intensity Cu rotating anode generator and a parallel beam multilayer mirror (CuKα1 radiation, λ = 1.540593 Å and CuKα2 radiation, λ = 1.544414 Å). Samples were scanned continuously at 45 kV x 160 mA, a step size of 2θ = 0.03 degree (3 s per step) over a 2θ range of 5 to 30 degrees. Thin film samples were prepared by drop casting 0.5 mg/ml solution of the isosceles triangles in CH_2Cl_2 onto piranha-cleaned Si wafer.

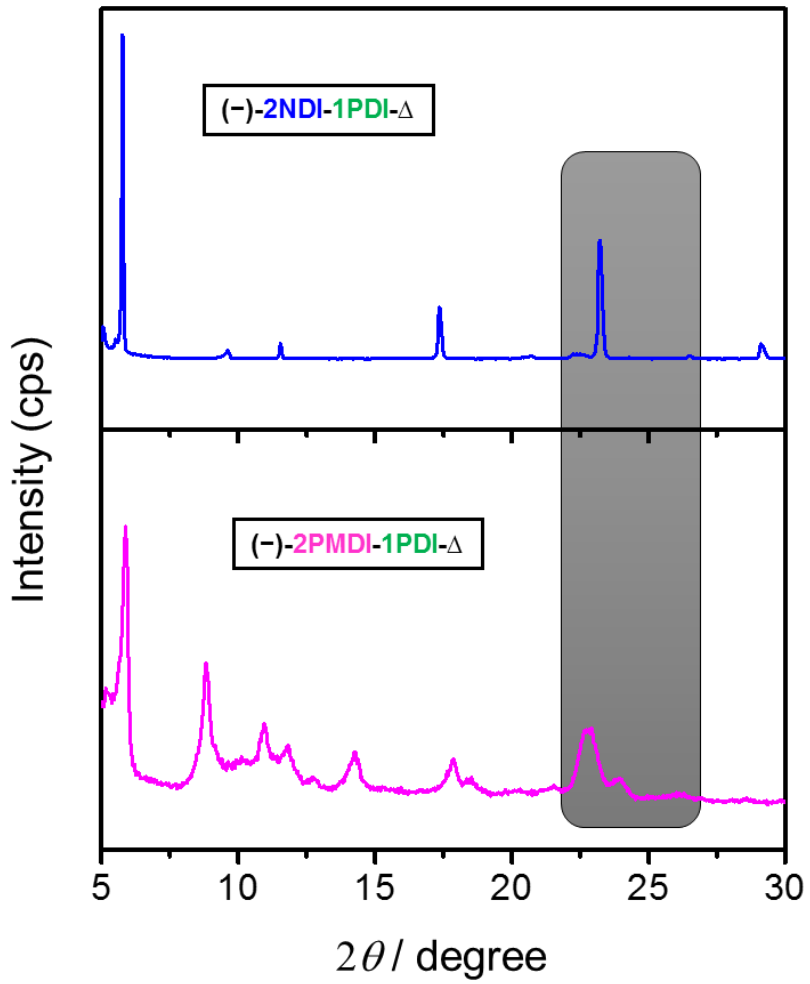

Figure S25. XRD patterns of the thin film samples prepared by drop casting CH_2Cl_2 solution of **(−)-2NDI-1PDI-Δ** (top) and **(−)-2PMDI-1PDI-Δ** (bottom) onto piranha-cleaned Si wafer. The highlighted region may suggest the possible intermolecular π-π stacking within the range of 3.2 to 3.7 Å between the curved, yet nearly co-facial, PDI units of the isosceles triangles. .

Section O. Time-resolved photoluminescence spectra

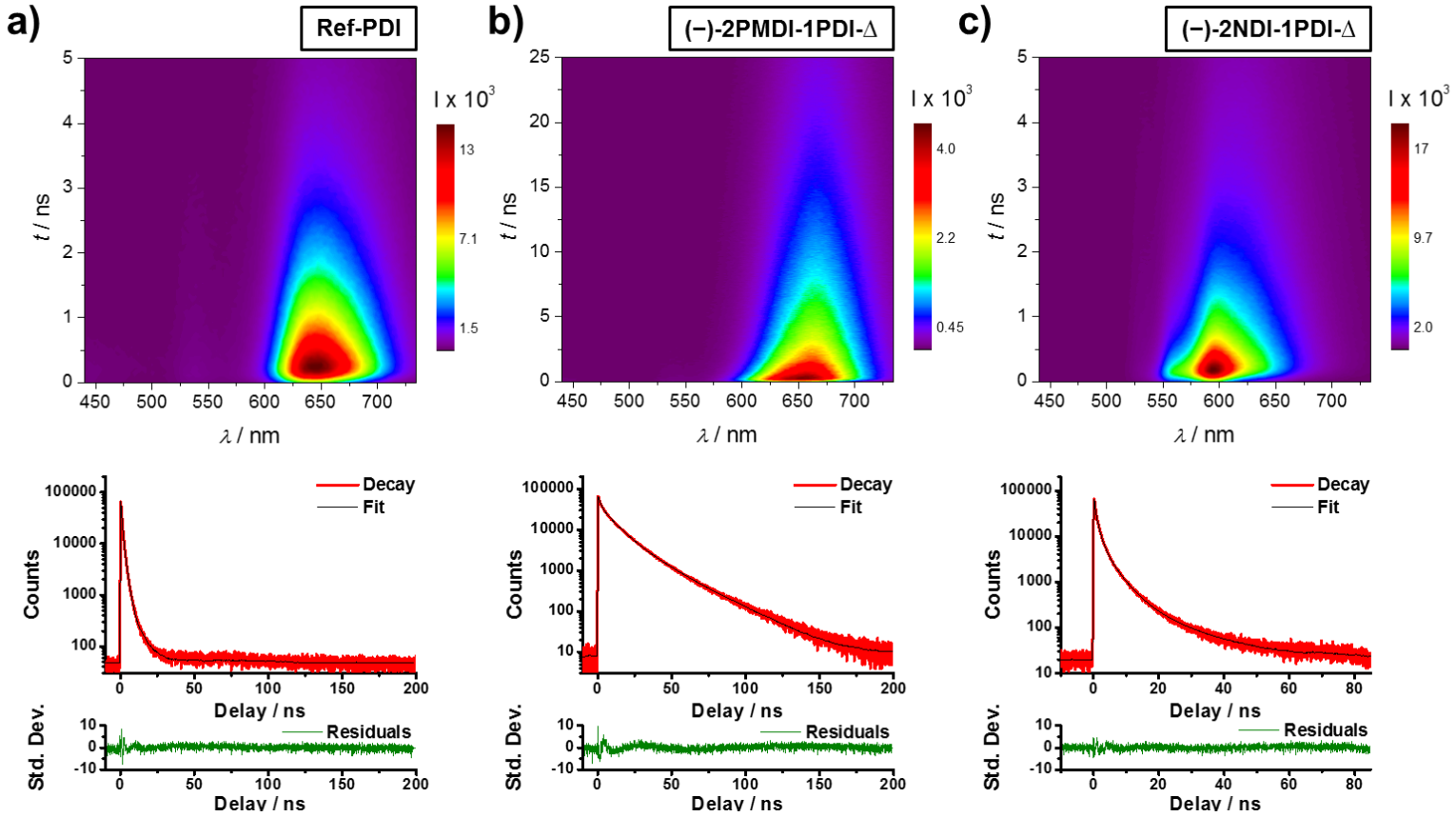

Figure S26. (**a**–**c**) Time-resolved photoluminescence spectra of **Ref-PDI** (**a**), **(−)-2PMDI-1PDI-Δ** (**b**) and **(−)-2NDI-1PDI-Δ** (**c**) recorded in the solid state at 298 K. The corresponding solid-state photoluminescence decay curves and the residuals are shown underneath. The photoluminescence spectra of all three compounds were measured in powder form with the excitation at 374 nm.

Section P. Time-dependent DFTB (TD-DFTB) calculations

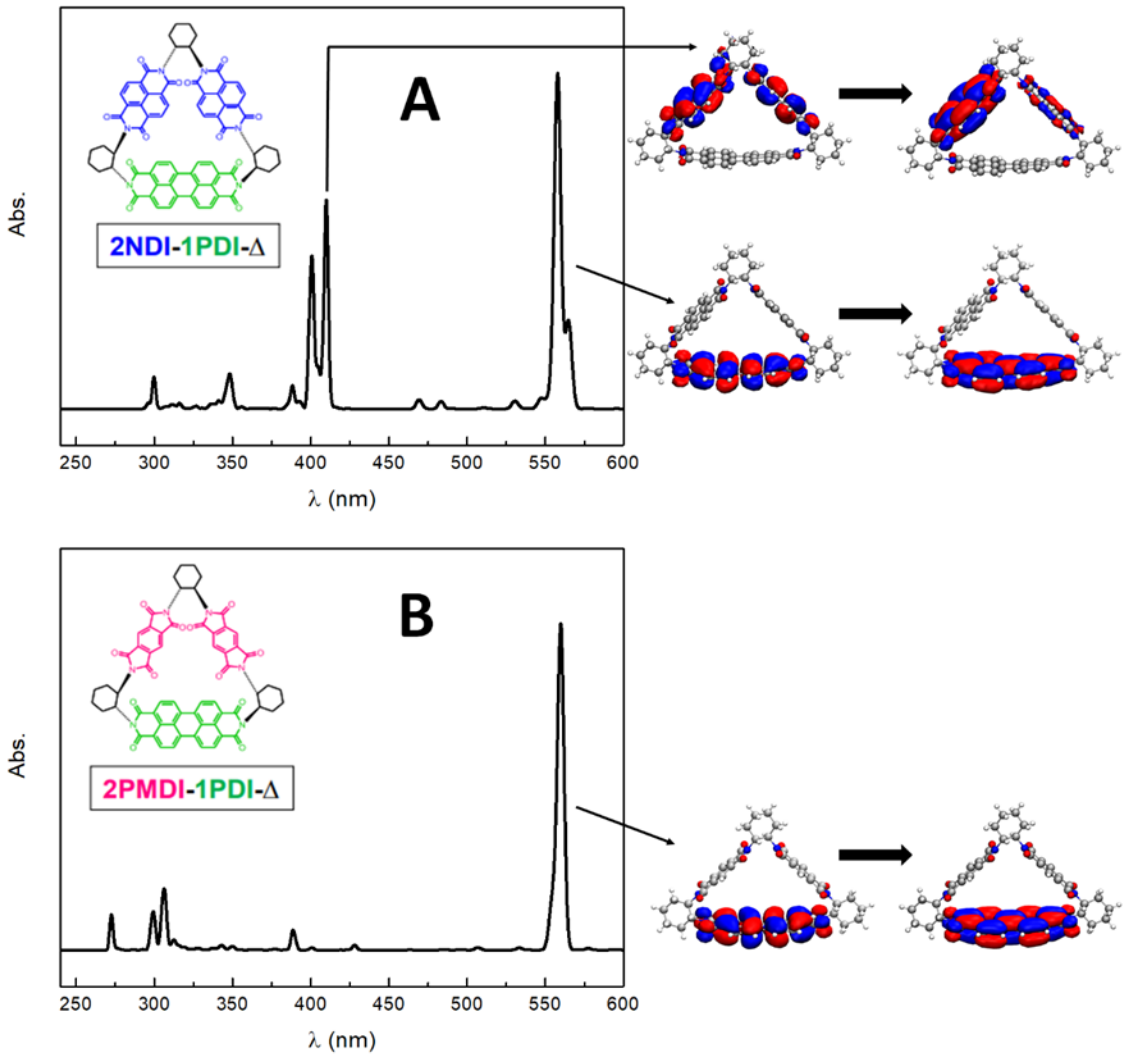

Figure S27. Simulated UV/Vis spectra of (a) **(−)-2NDI-1PDI-Δ** and the corresponding HOMO–LUMO electronic transitions at 400 and 560 nm, (b) **(−)-2PMDI-1PDI-Δ** and the corresponding HOMO–LUMO electronic transitions at 560 nm. Please note that the calculated wavelengths for the HOMO–LUMO electronic transitions are longer than the experimental values, which is expected since TD-DFTB usually sub-estimates the eigenvalues.

Section Q. Cyclic Voltammetry (CV) and Differential pulse voltammetry (DPV)

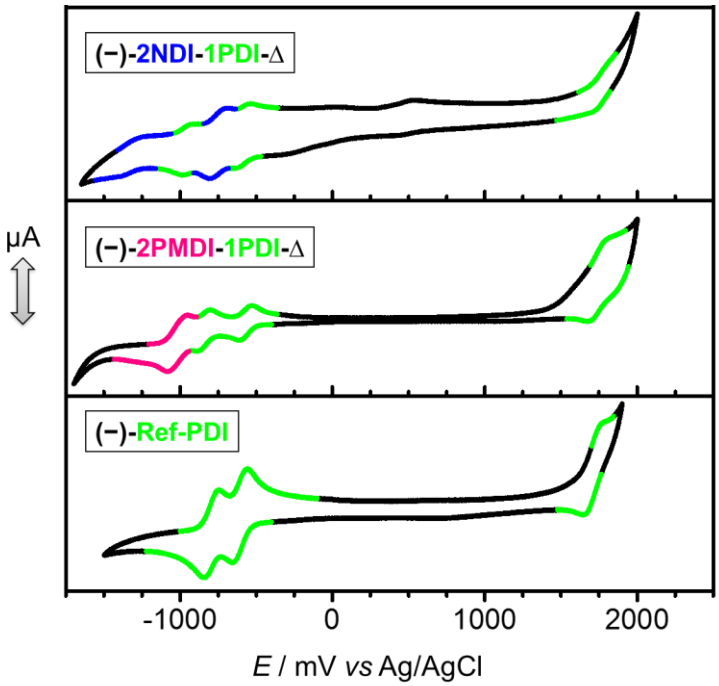

Figure S28. Cyclic Voltammograms (0.2 mM in CH_2Cl_2, 100 mM $TBAPF_6$, 50 mVs^{-1}, 298 K) of **Ref-PDI**, **(−)-2PMDI-1PDI-Δ** and **(−)-2NDI-1PDI-Δ**.

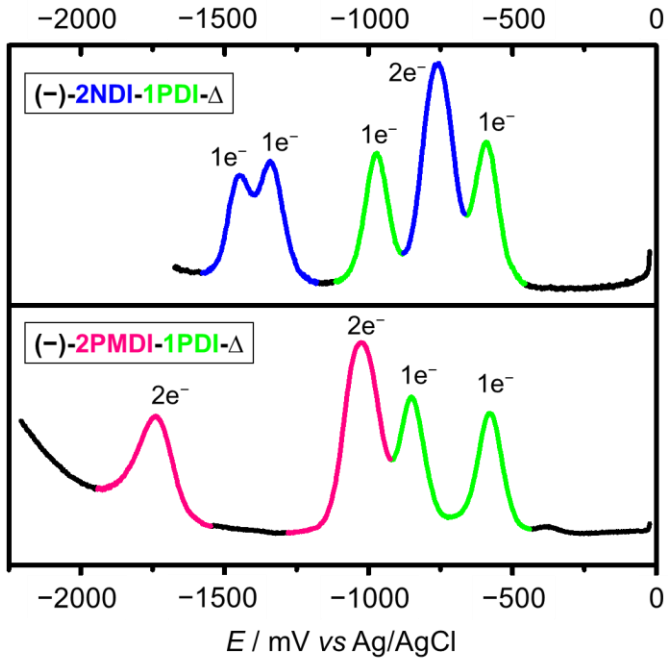

Figure S29. Differential pulse voltammetry (DPV) of the rigid isosceles triangles **(−)-2PMDI-1PDI-Δ** and **(−)-2NDI-1PDI-Δ** in CH_2Cl_2 (100 mM $TBAPF_6$, 50 mVs^{-1}, 298 K).

Section R. Spectroelectrochemistry

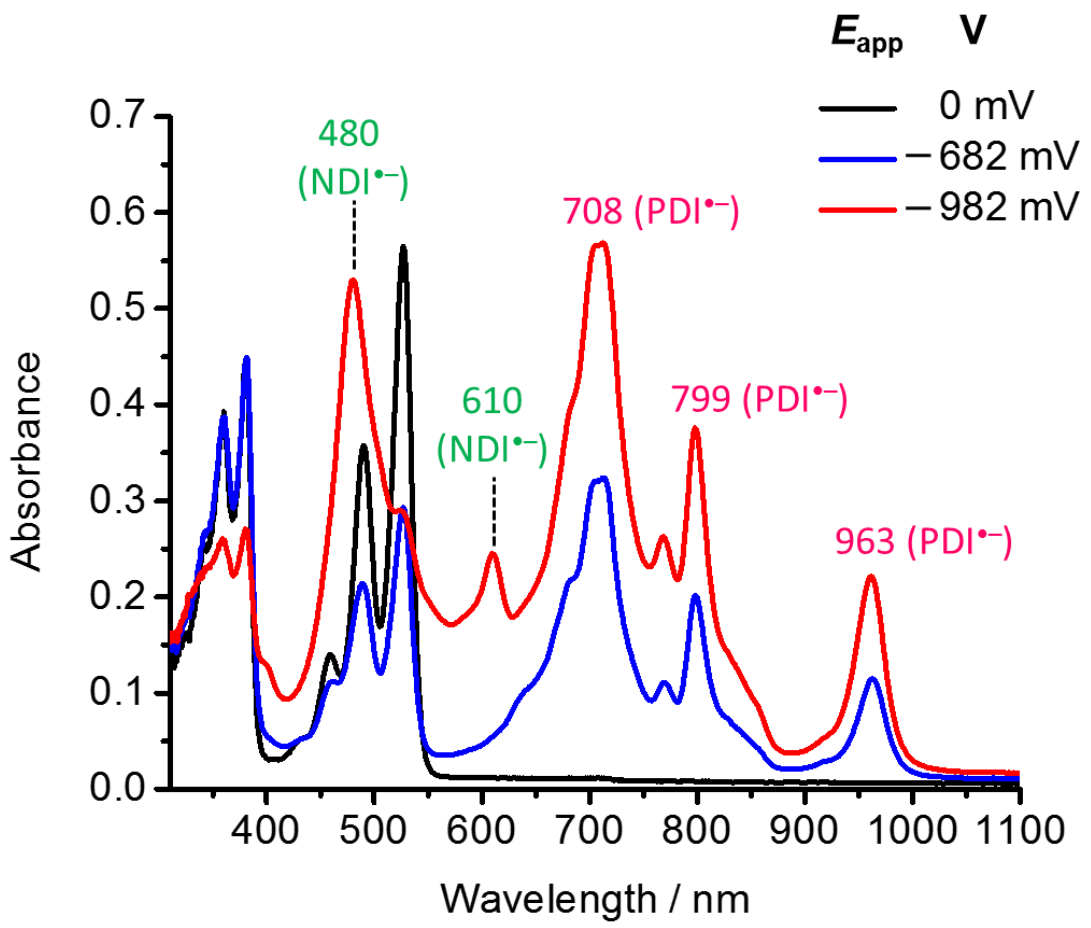

Figure S30. UV/Vis/NIR spectroelectrochemistry of **(−)-2NDI-1PDI-Δ** (10 μM in CH_2Cl_2, 100 mM $TBAPF_6$, 298 K) and the reduced states arising from the electrochemical reduction at different applied potentials (E_{app}).

Section S. EPR and ENDOR Spectroscopies

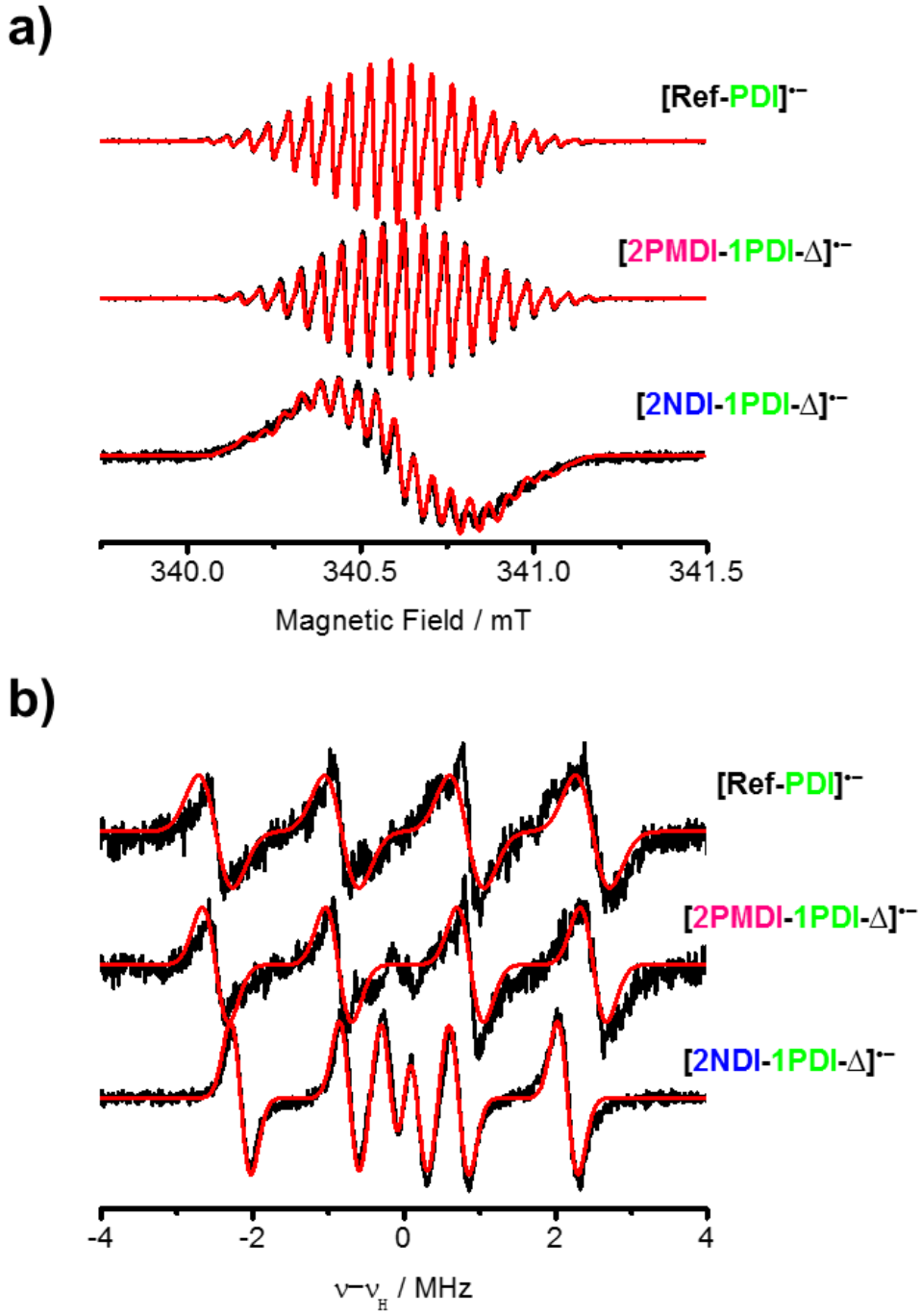

Figure S31. a) CW-EPR and b) ^{1}H ENDOR spectra (0.25 mM in CH_2Cl_2, 298 K) of [**Ref-PDI**]$^{\bullet-}$, **[(−)-2PMDI-1PDI-Δ]**$^{\bullet-}$ and **[(−)-2NDI-1PDI-Δ]**$^{\bullet-}$, formed by the monoreduction of their corresponding neutral states by adding 1 mol equiv of cobaltocene. Overlay between the experimental spectra (black traces) and their simulated spectra (red traces).

Section T. Supplementary references

1. Yu, L.; Li, P., New Simple Primary Amine–Thiourea Organocatalysts and their Application in Asymmetric Conjugate Addition. *Tetrahedron Lett.* **2014,** *55*, 3697-3700.
2. Schneebeli, S. T.; Frasconi, M.; Liu, Z.; Wu, Y.; Gardner, D. M.; Strutt, N. L.; Cheng, C.; Carmieli, R.; Wasielewski, M. R.; Stoddart, J. F., Electron Sharing and Anion–π Recognition in Molecular Triangular Prisms. *Angew. Chem., Int. Ed.* **2013,** *52*, 13100-13104.
3. Gawroński, J.; Brzostowska, M.; Gawrońska, K.; Koput, J.; Rychlewska, U.; Skowronek, P.; Nordén, B., Novel Chiral Pyromellitdiimide (1,2,4,5-Benzenetetracarboxydiimide) Dimers and Trimers: Exploring Their Structure, Electronic Transitions, and Exciton Coupling. *Chem. Eur. J.* **2002,** *8*, 2484-2494.
4. Nalluri, S. K. M.; Liu, Z.; Wu, Y.; Hermann, K. R.; Samanta, A.; Kim, D. J.; Krzyaniak, M. D.; Wasielewski, M. R.; Stoddart, J. F., Chiral Redox-Active Isosceles Triangles. *J. Am. Chem. Soc.* **2016,** *138*, 5968-5977.
5. Wu, Y.; Nalluri, S. K. M.; Young, R. M.; Krzyaniak, M. D.; Margulies, E. A.; Stoddart, J. F.; Wasielewski, M. R., Charge and Spin Transport in an Organic Molecular Square. *Angew. Chem., Int. Ed.* **2015,** *54*, 11971-11977.
6. Chen, Z. J.; Wang, L. M.; Zou, G.; Zhang, L.; Zhang, G. J.; Cai, X. F.; Teng, M. S., Colorimetric and Ratiometric Fluorescent Chemosensor for Fluoride Ion based on Perylene Diimide Derivatives. *Dyes Pigm.* **2012,** *94*, 410-415.
7. Shukla, D.; Nelson, S. F.; Freeman, D. C.; Rajeswaran, M.; Ahearn, W. G.; Meyer, D. M.; Carey, J. T., Thin-Film Morphology Control in Naphthalene-Diimide-Based Semiconductors: High Mobility n-Type Semiconductor for Organic Thin-Film Transistors. *Chem. Mater.* **2008,** *20*, 7486-7491.
8. Gawroński, J.; Brzostowska, M.; Kacprzak, K.; Kołbon, H.; Skowronek, P., Chirality Of Aromatic Bis-Imides from their Circular Dichroism Spectra. *Chirality* **2000,** *12*, 263-268.
9. Larrow, J.; Jacobsen, E., (R, R)-N, N'-Bis (3, 5-Di-Tert-Butylsalicylidene)-1, 2-Cyclohexanediamino Manganese (Iii) Chloride, A Highly Enantioselective Epoxidation Catalyst:(Manganese, Chloro 2, 2'-1, 2-Cyclohexanediylbis (Nitrilomethylidyne)-Bis 4,

6-Bis (1, 1-Dimethylethyl) Phenalato (2-)-N, N', O, O'-, Sp-5-1 3-(1 R-Trans--). *Org. Synth.* **1998,** *75*, 1-11.

10. Zhao, Y.; Truhlar, D. G., Density Functionals with Broad Applicability in Chemistry. *Acc. Chem. Res.* **2008,** *41*, 157-167.
11. Zhao, Y.; Truhlar, D. G., The M06 suite of density functionals for main group thermochemistry, thermochemical kinetics, noncovalent interactions, excited states, and transition elements: two new functionals and systematic testing of four M06-class functionals and 12 other functionals. *Theor. Chem. Acc.* **2008,** *120*, 215-241.
12. Goerigk, L.; Grimme, S., A Thorough Benchmark of Density Functional Methods for General Main Group Thermochemistry, Kinetics, and Noncovalent Interactions. *Phys. Chem. Chem. Phys.* **2011,** *13*, 6670-6688.
13. Grimme, S.; Antony, J.; Ehrlich, S.; Krieg, H., A Consistent and Accurate Ab Initio Parametrization of Density Functional Dispersion Correction (DFT-D) for the 94 Elements H-Pu. *J. Chem. Phys.* **2010,** *132*, 154104.
14. Rüger, R.; Lenthe, E. v.; Heine, T.; Visscher, L., Tight-Binding Approximations to Time-Dependent Density Functional Theory — A Fast Approach for the Calculation of Electronically Excited States. *J. Chem. Phys.* **2016,** *144*, 184103.
15. Dolomanov, O. V.; Bourhis, L. J.; Gildea, R. J.; Howard, J. A. K.; Puschmann, H., OLEX2: A Complete Structure Solution, Refinement and Analysis Program. *J. Appl. Crystallogr.* **2009,** *42*, 339-341.
16. Sheldrick, G., SHELXT - Integrated Space-Group and Crystal-Structure Determination. *Acta. Cryst. A* **2015,** *71*, 3-8.
17. Sheldrick, G. M., Crystal Structure Refinement with SHELXL. *Acta Cryst. C* **2015,** *71*, 3-8.
18. Thorn, A.; Dittrich, B.; Sheldrick, G. M., Enhanced Rigid-Bond Restraints. *Acta. Cryst. A* **2012,** *68*, 448-451.
19. Sheldrick, G., A Short History of SHELX. *Acta. Cryst. A* **2008,** *64*, 112-122.
20. Turner, M. J.; McKinnon, J. J.; Wolff, S. K.; Grimwood, D. J.; Spackman, P. R.; Jayatilaka, D.; Spackman, M. A., *CrystalExplorer17*. University of Western Australia: 2017.